Performance Analysis of Propagation Path Loss Model for Millimeter Wave Systems in Dense Urban Environments

Gezahegn Kushu Wami

A Thesis Submitted to

The Department of Electronics and Communication Engineering

School of Electrical Engineering and Computing

Presented in Partial Fulfillment of the Requirement for the Degree of Master's in Electronics and Communication Engineering

Office of Graduate Studies

Adama Science and Technology University

July, 2021

Adama, Ethiopia

Performance Analysis of Propagation Path Loss Model for Millimeter Wave Systems in Dense Urban Environments

By

Gezahegn Kushu Wami

Advisor: Dr. Satyasis Mishra

Co-Advisor: Dr. Demissie Jobir Gelmecha

A Thesis Submitted to
The department of Electronics and Communication Engineering

School of Electrical Engineering and Computing
School of Electronics and Communication Engineering

Presented in Partial Fulfillment of the Requirement for the Degree of Master's in Electronics and Communication Engineering

Office of Graduate Studies
Adama Science and Technology University

July, 2021
Adama, Ethiopia

APPROVAL PAGE OF M.SC. THESIS

We, the advisors of the thesis entitled "Performance Analysis of Propagation Path Loss Model for Millimeter Wave System in Dense Urban Environments" and developed by Gezahegn Kushu, hereby certify that the recommendation and suggestions made by the board of examiners are appropriately incorporated into the final version of the thesis.

______________________	______________________	______________
Advisor	Signature	Date
______________________	______________________	______________
Co-Advisor	Signature	Date

We, the undersigned, members of the Board of Examiners of the thesis by Gezahegn Kushu have read and evaluated the thesis entitled "Performance Analysis of Propagation Path Loss Model for Millimeter Wave System in Dense Urban Environments" and examined the candidate during open defense. This is, therefore, to certify that the thesis is accepted for partial fulfillment of the requirement of the degree of Master of Science in Electronics and Communication Engineering

______________________	______________________	______________
Chairperson	Signature	Date
______________________	______________________	______________
Internal Examiner	Signature	Date
______________________	______________________	______________
External Examiner	Signature	Date

Finally, approval and acceptance of the thesis is contingent upon submission of its final copy to the Office of Postgraduate Studies (OPGS) through the Department Graduate Council (DGC) and School Graduate Committee (SGC).

______________________	______________________	______________
Department Head	Signature	Date
______________________	______________________	______________
School Dean	Signature	Date
______________________	______________________	______________
Office of Postgraduate Studies, Dean	Signature	Date

DECLARATION

I hereby declare that this Master Thesis entitled "Performance Analysis of Propagation Path Loss Model for Millimeter Wave System in Dense Urban Environments" is my original work. That is, it has not been submitted for the award of any academic degree, diploma or certificate in any other university. All sources of materials that are used for this thesis have been duly acknowledged through citation.

______________________	______________________	______________
Name of the student	Signature	Date

RECOMMENDATION

We, the advisors of this thesis, hereby certify that we have read the revised version of the thesis entitled "Performance Analysis of Propagation Path Loss Model for Millimeter Wave System in Dense Urban Environments" prepared under our guidance by Gezahegn Kushu submitted in partial fulfillment of the requirements for the degree of Masters of Science in Electronics and Communication Engineering. Therefore, we recommend the submission of revised version of the thesis to the department following the applicable procedures.

______________________	______________________	______________
Advisor	Signature	Date
______________________	______________________	______________
Co-Advisor	Signature	Date

ACKNOWLEDGEMENT

I would like to gratefully acknowledge my advisor Dr. Satyasis Mishra, ASTU. Adama, Ethiopia for his continuous encouragement throughout the research work. As well as wisher, his insight, observations and suggestion help as to establish the overall direction of the research and contributed immediately to the success of the work.

I would like greatfully acknowledge my co-advisor Dr. Demissie Jobir Gelmecha, ASTU. Adama, Ethiopia for their support and suggestion during the final phase of the preparation of the report .as well as his hospitality.

Finally, I would want to express my gratitude to my family, particularly my wife, Meseret Tefera, for her moral support and sacrifices made throughout my studies. Her compassion, generosity, concern, and prayers provided me with the motivation to accomplish my course work and thesis.

TABLE OF CONTENTS

LIST OF TABLES

LIST OF FIGURES

LIST OF ABBREVIATIONS

1G	First Generation Wireless Systems
2G	Second Generation Wireless Systems
3G	Third Generation Wireless Systems
4G	Fourth Generation Wireless Systems
5G	Fifth Generation Wireless System
5GCM	5G Channel Model
3GPP	3^{rd} Generation Project Partnership
5GMF	5G Mobile Communication Promotion Forum
5GPPP	5G Infrastructure Public Private Partnership
ABG	Alpha-Beta-Gamma
BER	Bit Error Rate
BPL	Building Penetration Loss
BS	Base Station
CDMA	Code Division Multiple Access
CI	Close-In
dB	Decibels
dBi	dB gain with respect to isotropic antenna
dBm	dB respect to one mill watt
DL	Downlink
DVB	Digital Video Broadcasting
EDGE	Enhanced Data Rate for GSM Evolution
EMBB	Enhanced Mobile Broadband
ETSI	European Telecommunication Standards Institute
EHF	Extremely High Frequency
FSL	Free Space Loss
Gbps	Giga Bits per Seconds
GPRS	General Packet Radio Service
GHz	Giga hertz
GSM	Global System for Mobile Communication

HBF	Hybrid Beamforming
HPBW	Half-power beam width
HSDP	High Speed Downlink
HSUP	High Speed Uplink
IMT-2020	International Mobile Telecommunication-2020
IOT	Internet Of The Things
ISD	Inter Site Distance
ITU-R	International Telecommunication Recommendation
KPI	Key Performance Indices
LAN	Local Area Network
LOS	Line of Sight
LTE	Long Term Evolution
LTE-A	LTE-Advanced
Mbps	Megabits per Seconds
MHz	Mega hertz
MIMO	Multiple-Input-Multiple-Output
MMS	Multimedia Messaging Service
MMSE	Minimum Mean Square Error
mmwave	Millimeter Wave
MPC	Multipath Components
PDP	Power Delay Profile
O2I	Outdoor-to-Indoor
OFDM	Orthogonal Frequency Division Multiplexing
NLOS	Non-Line of Sight
PL	Path Loss
PLE	Path Loss Exponent
QAM	Quadrature Amplitude modulation
QPSK	Quadrature Phase Shift Keying
QoS	Quality of Service
RAT	Radio Access Technology
RxS	Receiver Sensitivity

RxSL	Received Signal Level
SINR	Signal-To-Interference-Plus-Noise Ratio
SMS	Short Messaging Service
SNR	Signal-To-Noise Ratio
TX	Transmitter
UMa	Urban Macro
UMi	Urban Micro
WLAN	Wireless Local Area Network

LIST OF SYMBOLS

P_R	Power of Received Signal
P_T	Power of transmitted
P_d	Power Density
G_T	Antenna Gain Of Transmitter
G_R	Antenna Gain Of Receiver
Λ	Intensity
σ	Standard Deviation
f	Frequency
λ	Wavelength
E	Electric Field
H	Magnetic Field
$\bar{\tau}$	Average Excess Delay
$\sigma\tau$	RNS Delay Spread
n	Path Loss Exponent
X_σ	Zero Mean Gaussian Random Variable
α	Floating Intercept
β	Slop Of Fitting Line
θ_k	Angle Above Pre-Define Threshold Value
I	Interference Signal
N	Noise Power Received
f_c	Carrier Frequency
Ψ	Set Of Base Station
(R_ℓ, φ_ℓ)	Polar Coordinate of The Base Station bl in x-y plane
vi	speed of user over i^{th} interval
τi	Duration of i^{th} interval
β_i	Parameters of τ_i for exponential distribution
g_ℓ	Gamma random variable

M	Main Lobe
m	Back Lobe Directivity
θ	Beam Width of Main Lobe
ϕ_U	Arrival angle of the signal of the link
ϕ_B	Departure angle of the signal of the link
$G0$	Directivity gain of labeled BS link
r_ℓ,	Distance Between the BS and user
α_ℓ	Power Loss Exponent
p_ℓ	ABG path loss
σN^2	Additive Power Of Noise
B_W	User Bandwidth
N_F	Noise Figure in dB
L	Length of Blockings

ABSTRACT

A number of studies on future mobile communications, millimeter wave (mmwave) has been identified as a crucial enabling technology for achieving massive connectivity in the Fifth generation (5G) and beyond periods. However, millimeter wave propagating signals suffer from high propagation loss and sensitivity to blockage, resulting in high outage probability and low Signal-to-Noise Ratio (SNR). This thesis analysis the performance of millimeter wave propagation path loss and building penetration loss (BPL). The loss is crucial for understanding the huge impact on many important things in Radio Access Network (RAN) and network performance. The Close-n (CI) Reference Model, and the Alpha-Beta-Gamma (ABG) Model are among the path loss models. They have high consistency and accuracy, and are acceptable for urban areas and outdoor to indoor scenarios in the 5G Channel Model (5GCM). We discussed the results of simulations at 4 GHz, 28 GHz and 73 GHz for 5G cellular networks in dense urban environments. Simulations are performed with the MATLAB 2017a program to analysis the performance of mm wave characterization. Our thesis presents large-scale characterization of mm wave such as path loss, delay spread, and power delay profile and also BPL for both line-of-sight (LOS) and non-lime-of-sight (NLOS) cases. The thesis also analysis propagation of directional and omnidirectional path loss in smaller microcells with five times larger cell size to performance difference and the effects of various millimeter wave frequency bands with the increase in transmitter (T_X) and receiver (R_X) distance. At high frequency, both low BPL and high BPL performance gradually decline when the distance between base stations (BSs) and user's increases. Our work shows that mm wave communications is feasible for all fifth generation (5G) deployments within the range of microcells of 200m and 112m for frequencies such as 28 GHz and 73 GHz respectively, and for macrocells in the range of 625m for lower frequencies such as 4 GHz to be used in dense urban areas.

Keywords*: Millimeter Wave Communication, Dense Urban Networks, Fifth Generation (5G) Channel Model, Path Loss.*

CHAPTER ONE

1. INTRODUCTION

1.1 Background of the Study

Nowadays, mobile communication is extremely vital. Existing wireless communication and future mmwave cellular communication have differences in directivity, propagation loss, and sensitivity to obstruction [1, 2]. The obstruction to fully exploiting the capability of mmwave communication serves massive connectivity, especially in urban environments [3, 4]. The need for heterogeneous networks such as 5G, in dense urban environments, appears to be characterized by a growing number of connected devices, heavy traffic load, outdoor, and outdoor to indoor [5]. Several constraints further limit the deployment of 5G mmwave networks in the era. The availability of buildings made out of concrete, bricks, glass, wood, and others, as well as the hard features of mmwave for penetrating these materials [6].

Many developing countries have implemented Fourth Generation (4G) or Long Term Evolution (LTE) technology, and 5G technology in 2020 [7]. The researchers realized that frequency bands lower than 6GHz are already fully occupied with other applications. Hence, the new spectrum range needs 5G technology. Path loss is a major limiting factor in reducing the receive power and network performance in wireless communication. Some popular models, such as the "Hata Model, Okumura Model, and Lee Model" are applicable between 200MHz and 2000MHz. The millimeter wave is the wavelength which needs to be accessed by mobile stations (MS).The frequency range will be from 3 GHz to 300 GHz. The path loss parameters for millimeter wave frequency analysis is one aspect of this research. The technique being used is by measuring received signals in dense urban areas for LOS conditions.

Three path loss models have been discussed. The first one is known as the Close-In reference model that is used for LOS conditions and outdoor scenarios. The second is the close-in with a frequency weighted or height weighted path loss exponent (CIF) used for indoor scenarios, and the third is the floating intercept (FI) or Alpha-Beta-Gamma Model or ABG Model, which is used for urban microcells (UMi) NLOS and outdoor-to-indoor scenarios [8] as well as for NLOS conditions. The close-in model was chosen for modeling UMi NLOS path loss. The

ABG model is very nearly identical to the CI model [9]. Some techniques, such as adaptive power control, adaptive transmission control, and diversity protection schemes, have been proposed [10]. In urban cellular networks, the cell size of the 5G network is expected to be smaller compared to previous generations due to the implementation of higher frequency. Thus, the radius of the cell for the 5G network is expected to be about 200 meters [11]. However, since the range of millimeter waves is wide (273 GHz), the cell size at the lower frequency of millimeter waves is much wider.

The aim of this thesis is to identify innovative solutions for 5G mmwave systems and applications that deal with severe attenuation and restricted propagation characterization. Large-scale fading of mmwave 5G system propagation with huge Multiple Input Multiple Output (MIMO) antennas in dense urban areas, as well as the propagation analysis in the 4 GHz, 28 GHz, and 73 GHz frequency bands and penetration loss of buildings for 5G networks [12, 13].

1.2 Statement of the Problem

Millimeter wave frequency ranges from 3 GHz to 300 GHz, with wavelengths ranging from 100mm to 1mm. Any parameters must be determined for various environments due to the short wavelength. The short wavelength frequency has enormous limitations compared to the longer one in the free space propagation environment. The distance for millimeter waves is shorter for the same value of transmit power. It reflects the smaller cell sizes it is capable of producing. Increasing the transmit power is not a good solution because it would increase the service provider's running costs and efforts.

Path loss is a factor that influences both cell size and distance. The path loss is traditionally measured using two physical parameters: frequency and distance. The old model can be reliable for frequencies less than 3 GHz, but due to the shorter wave length and much broader frequency band, it is less effective for millimeter waves. In order to predict the millimeter wave signal strength at a given distance, high-accuracy and consistency path loss models are needed. As a result, reduce higher Doppler spread and heavy attenuations in mmWaves using directional antennas, as compared to massive MIMO or huge antenna arrays when channel modeling.

1.3 Objectives of Thesis

1.3.1 General Objective

Analysis the performance for outdoor-to-indoor mm wave propagation for dense urban 5G cellular networks in terms of propagation path loss and building penetration loss.

1.3.2 Specific Objectives

The specific objectives of this thesis will be achieved through the following:

- For analysis, millimeter wave path loss models are currently available.
- The 5GCM model has higher accuracy and LOS probability than other channel modeling for mmWaves using stochastic channel models, due to lower computational complexity, and is suitable for system design.
- Analysis of suitable channel models based on simulated results.
- By knowing the number of gNodeB, the vendor and operator will be able to estimate the cost and operation when the path loss is analyzed.
- Analysis of the capacity achieved based on various quality requirements.

1.4. Scope of thesis

The scope of this thesis is primarily concerned with outdoor-to-indoor scenarios propagation path loss models for millimeter wave systems in dense urban environments. The following are the components of this thesis scope:

- The recommended bandwidth of 200 MHz for 4 GHz and 800 MHz for 28 GHz and 73GHz 5G systems will be used.
- Cell size is evaluated using the ABG path loss model.
- For the number of gnodeB known, we used Adama city coverage area by taking from the land administration by hectare 22165 or 221 km square.
- The measurement will be carried out in an outdoor-to-indoor environment within dense urban area by the prospective candidate. The value of each parameter that is used for analysis simulation results is 28 GHz bands, but we used 4 GHz and 73 GHz bands.

1.5 Contributions of Thesis

- To analyze the large scale fading such as path loss, delay spreads and shadow factor of propagation at mmwave bands and the performance of 5G networks, we utilize MATLAB simulations.
- The analysis of 4 GHz propagation for 5G networks, Although 4 GHz has already been used in some applications, the 5G system will see huge bands in the sub-6 GHz frequency bands.

1.6 Organization of Thesis

The following chapters for this thesis are arranged based on Chapter One.

- Chapter two: There is an overview of the literature on the evolution of developing cellular networks. The evolution of communication systems over the last few years will be addressed, followed by an overview of 5G cellular networks. Following that, the dense urban environment and its significant for 5G systems are discussed. The millimeter wave is important as an enabling technology and the propagation characteristics of 5G bands are also discussed. The millimeter wave spectrum is discussed, as well as the propagation characteristics of mmWaves, including atmospheric impacts. At mmWaves, free space path loss, atmospheric losses, rain attenuation, and material penetration are covered.
- Chapter 3: Millimeter Wave channel models and systems are discussed. The efforts and challenges of mmWave channel modeling are discussed, followed by an overview of the system design considerations, model, and link budget calculation scenarios used in this thesis.
- Chapter 4: shows simulation results at 4 GHz, 28 GHz, and 73 GHz bands for 5G urban dense networks. The simulation results for UMi and Urban Macrocell (UMa) are described in detail, and various scenarios, such as LOS and NLOS performance of the listed frequency bands, as well as penetration loss with blockage intensity at 28 GHz, are discussed. Finally, they draw a conclusion based on simulation results and give a thesis direction at the conclusion.

CHAPTER TWO

2. LITERATURE REVIEW

2.1 Development of Wireless Communication

Long before the industrial revolution, the first wireless networks were developed using smoke signals, flashing mirrors, or semaphore flags, among other methods. Guglielmo Marconi demonstrated the first radio transmission more than a century ago, in the mid-1890s, and the era of radio communication began [14]. Wireless communications have continued to change since then, with new ways and systems being deployed. After the beginning of the cellular concept and advancements in radio frequency hardware in the 1960s and 1970s, a new era of wireless communication began [14].

Nowadays, wireless communication is the fastest increasing engineering field with its wide spread applications overcame in all aspects of 21th century human kind life. T.S. Eliot claims that According to Rappaport et al. in [3] every 10 years has seen a new generation of wireless communication systems with more advanced technology in terms of data rate, spectrum efficiency, coverage, and applications from the dawn of the new era in 1980.

Although early wireless Local Area Networks (LANs) could not compete with wired Ethernet technology, the most successful application of wireless communication has been the cellular systems [15]. The first generation (1G) cellular system, which was an analog system with a few kbps data rates and a number of drawbacks, was announced in the early 1980s. The famous 2G technologies were the "Global System for Mobile Communications (GSM)", and Upgrades to 2G, such as General Packet Radio Service (GPRS) and Enhanced Data Rate for GSM Evolution (EDGE), increased the data rate to 144 kbps and 384 kbps, respectively [2].

In 2000, the third generation was released, with new technologies and features. The initial transmission rate was 2Mbps, but as new technologies such as High-Speed Uplink/Downlink Packet Access (HSUPA/HSDP) were added to the network, it was increased to 30Mbps [2]. Long Term Evolution (LTE) technology was introduced by the 3rd Generation Project Partnership (3GPP) as a descendant of previous cellular generations, which is referred to as 4G, and was followed by LTE-Advanced, which has an even higher bit rate. 5G, a new generation of cellular networks addresses the exponential growth in demand for higher data traffic, as well as the other challenges 4G LTE is currently facing in terms of capacity, end-to-end latency, massive device connectivity, quality of service, and cost. Figure 2.1 from [2] depicts the progression from 1G to 4G. The next part will provide a clear explanation of 5G and how it will overcome the challenges that it will face in its deployment in figure 2.1.

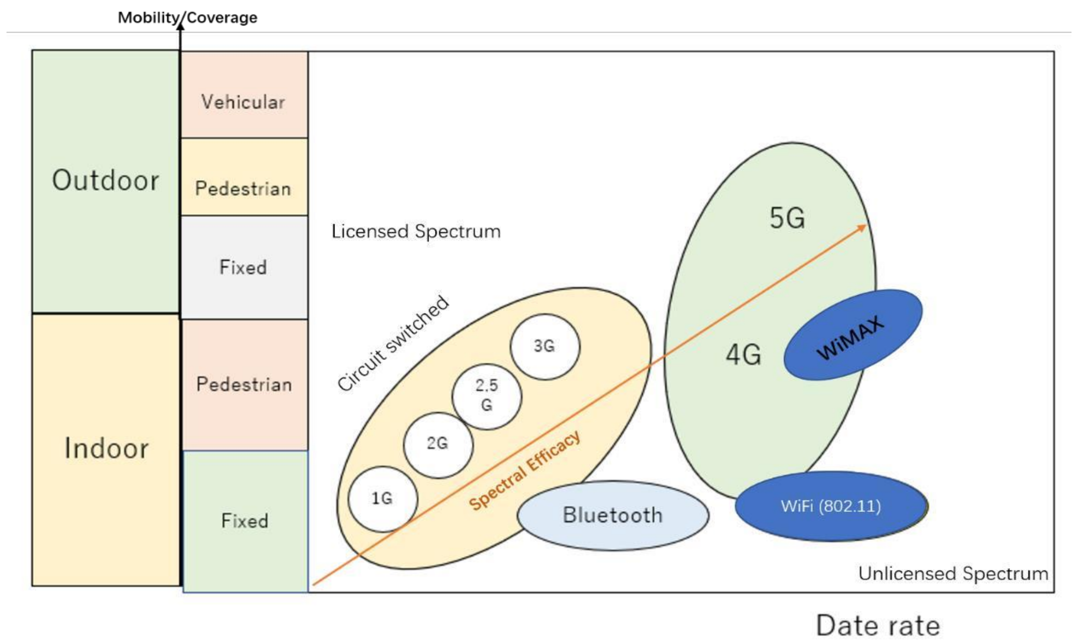

Figure 2.1: Evolution of cellular network and of wireless communications [2]

2.2 An Overview of 5G Cellular System

By the exponential increase in customer demand for new applications and services, 5G mobile systems are now being considered to meet the requirements of these services in terms of data latency, reliability, and throughput, as well as cheap price and huge connectivity [16].

Since then, several initiatives and projects have been launched around the world to investigate 5G and allowing technologies in the years ahead. In Europe, the “European Union framework program for research and innovation (Horizon 2020)” and “5G Infrastructure Public Private Partnership (5GPPP)” [17], research the “NYU WIRELESS center” [18], and “5G Infrastructure Public Private Partnership (5GPPP)” in the United States, the”IMT-2020 (5G) Promotion Group “in China [19], the” 5G Forum in Korea and the 5G Mobile Communications Promotion Forum(5GMF)” [13] in Japan have all actively promoted

5G research and development, while 3GPP [20] and other standardization bodies are finalizing the 5G NR and related standards.

To minimize the severe propagation characteristics of mmWaves for 5G, researchers proposed beamforming (BF) and large Multiple-Input and Multiple-Output (MIMO) using highly directed antenna arrays. [21, 22] discussed small cells with heterogeneous systems for 5G. In addition, network slicing for 5G was discussed in [23], and authors in [2] presented a general heterogeneous architecture for 5G cellular technologies, illustrating how heterogeneous network combining microcells, small cells, 5G Wi-Fi, D2D communication, wireless sensor networks, massive MIMO, and other technologies will be used for 5G. Several other researchers have proposed splitting indoor and outdoor setups for 5G, due to millimeter wave's high penetration losses [24]. Authors in [25] proposed low cost channel sounder and post processing methods that may be used to investigate 3D-MIMO channels and obtain elevation and azimuth parameters between 2.52 and 2.54 GHz in dense urban areas.

At higher frequency bands of outdoor-to-indoor (O2I) scenarios, this thesis analysis shows that the coverage varies over the frequency bands. Millimeter wave propagation, along with outdoor-to-indoor scenarios and building penetration loss, is a problem for mmwave deployment in 5G and beyond wireless networks. We will also utilize huge antenna arrays to emphasize directional transmission at mmwave frequencies in order to provide efficient beamforming techniques for minimizing directional propagation loss. In the next section below, we will describe how dense urban environments will be attractive for 5G and how mmwave will be crucial for 5G dense urban populated areas.

2.3 Dense Urban Deployments

With a density of 4-5 BSs/km^2, cellular network densification for 3G was designed to improve the transmission rate. Hotspot and femtocell BSs have been deployed at a density of 8-10 BSs/km^2 for 4G LTE-Advanced. The density of 5G is expected to reach 40-50 BSs/km^2 to meet the requirements of 5G and to benefit from massive MIMO and millimeter wave technologies, making it an ultra-dense cellular network [26].

The dense urban scenario is one of the 10 deployment scenarios explored by 3GPP [27], and it is one of the scenarios proposed for enhanced mobile broadband (eMBB). In this heterogeneous deployment scenario, large cells with micro cells in city centers and dense urban areas with high user densities are prioritized. The major characteristics of this situation are high traffic loads and outdoor and outdoor-to-indoor coverage. The macrocell Inter-Site-Distance (ISD) is 500 m in this case. Macro and micro cells have heights of 25 and 10 meters, respectively. The carrier frequency for macrocells is 4 GHz, while microcells have carrier frequencies of roughly 28 GHz and 73 GHz. The bandwidth for 4 GHz is up to 200 MHz, and for both 28 GHz and 73 GHz, it is up to 800 GHz.

2.4 Millimeter Wave as Key Enabling Technology

The global bandwidth shortage in sub-3 GHz bands, as well as the rapid development of wireless and mobile traffic, has exhilarated researchers to look into and use under-utilized millimeter wave spectrum to satisfy the needs of 5G and beyond networks [3, 28]. Massive MIMO With the large bandwidth of millimeter wave, along with significantly reduced antenna diameters that allow more antennas to be packed into a small printed circuit board, small packaging, or on a chip, enables high data rates that are essential in various 5G condition [29]. Many studies have looked into and demonstrated that mmWave utilized in different features of 5G, ranging from small cell connectivity to provide multi-gigabit transmission rates and cellular connectivity for high coverage and capacity when densely implemented, wireless backhaul replacing fiber-based backhauls while even preserve multiple Gbps data rates [21], despite the difficulties in fully utilizing the benefit of mmwave communication ,the provided solutions and planned system on mmwave are very promising ,providing mmwave crucial enabling technology for 5G and beyond networks.

2.5 Proposed Solution for 5G

The most important is 5G, which archives high data rate than LTE. Millimeter wave spectrum, small cells, and massive MIMO are three solution proposed 5G.

2.5.1 Millimeter Waves Spectrum

The microwave carrier frequency spectrum, which ranging 0.7 - 2.6 GHz and with bandwidth of less than 780 MHz, is currently used in public cellular wireless communications [26]. Since the wavelength of the spectrum is from 100 mm and 1 mm, there are much more frequency resources and bandwidth in the underdeveloped and underutilized high frequency spectrum ranging 3 -300 GHz, known as millimeter wave.

Potential available 252GHz bandwidth is large supply for many wireless application including the mobile broad band as shown in figure 2.2. since, oxygen absorption and water vapor in the atmosphere high attenuation [30] and there is a limitation propagation in portions of the spectrum, for mobile cellular network sub 100-GHz bands.

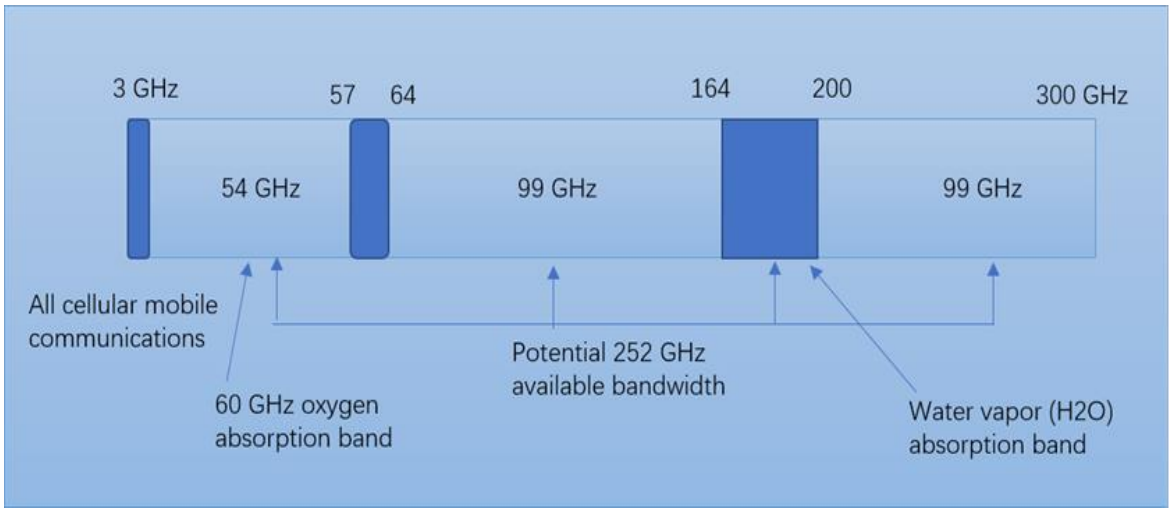

Figure 2.2: Millimeter wave spectrum, along oxygen and water vapor absorption bands [30]

The millimeter wave spectrum is divided and named into many bands based on the usage and wavelength of the sub-100 GHz bands. These bands are shown in Table 2.1 [24], along with their frequency ranges and wavelengths. Different countries have considered several applications in both of these bands. Satellite, astronomy, and terrestrial microwave communications all use the Q band, which ranges from 30 GHz to 50 GHz. 60 GHz is a portion of the V band that ranging from 50-75 GHz and is utilized for unlicensed wireless communications [31]. Standardization bodies have focused on some parts of the E band, such as 71-76 GHz, 81-86 GHz, and 92-96 GHz, for use in fronthaul and backhaul networks, especially in the united states [24]. Satellite communications and deep space research will also benefit from the W band, which has a short wavelength.

Table 2.1: Millimeter wave frequency band designation for sub-100GHz [24]

Design of band	Rang of frequency(in GHz)	Wavelength(mm)
Q	30-50	10.00-6.00
U	40-60	7.50-5.00
V	50-75	6.00-4.00
60-90	5.00-3.33	
75-110	4.00-2.73	

2.5.2 Small Cells

The capacity of the network effectively increase by Small cells [32]. Several kinds of cell dimensions can achieve different coverages and capacity of the network such as, microcells, picocells and femtocells [32]. By lowering the cell dimension, spectrum reuse can be done in a specific area. But at the same time, in a dense network signal-to-interference ratio (SIR) is increased [32]. The typical cellular communication uses macrocells cover large geographic areas with high capacity. For these macrocells, the antennas are typically mounted on the rooftops of tall buildings, or on tall towers, and transmit radio frequency (RF) signals at high power levels. However, macrocells do not provide the most desirable performance in every scenario. In order to address coverage and/or capacity challenges, there can be cells with different levels of capacities and sizes, for example, microcells, picocells, and femtocells. The term microcell is conventionally used to describe a single, outdoor, short-range radio transceiver. The cost of implementing small cells is major concern, increased cost of small cells networks is due to the needs for site permission, the requirements of reliable backhaul networks, and site rent.

2.5.3 Massive MIMO

Massive MIMO is the concepts of large scale antenna arrays. The base station in the system continue to be equivalent with high numbers of antenna connected to active users who were using each time-frequency signaling resource .if the number of users per supply is the tens, the number of antenna per base station will be in the hundreds. The following problems that massive

MIMO systems face: pilot transmission must be orthogonal among operators of the small cell and reused to offer clear channel estimation or otherwise all resource will be taken by pilots.

Even with the enormous numbers of antennas in BS, the interference known as pilot contamination there are design complexities for the vision of huge MIMO system. The sociability antenna condition and coupling ,price etc. are issue of massive MIMO architecture including high power amplifiers for sectors antenna and low power amplifiers for micro antennas[32].

Broad ranging field measurements are needed for channels models. For large antennas, antenna correlation and coupling should be analysis, actual channel orthogonally should be validated, and the channel models effects of channel model evaluated .if the network became dense with small cells, the necessity for massive MIMO system will vanished as the number of active user per cell decrease. This thesis considers mmwave networks to be crucial in staffing 5G scenarios.

2.6 Propagation Characteristics of mm Wave at 5G Bands

Millimeter wave frequencies are various propagation analyzation from sub-3 GHz bands. Furthermore, each frequency in the huge millimeter wave spectrum has various propagation; hence, analysis the propagation of candidate bands for 5G aids in a better grasp of mmwave and accurate modeling for various 5G implementation environments. We will go through the most important millimeter wave propagation characteristics, such as free space propagation, atmospheric losses, rain attenuation, material penetration, and reflection coefficients.

2.6.1 Free Space Propagation

To indicate that there are no obstacles between transmit and receive antennas in this form of propagation, the transmit antenna should be placed at a certain height above the ground surface**.** Assuming a transmit antenna gain is G_T, a receiver antenna gain is G_R, power of transmit is P_T, and the power receiver P_R at is given by.

$$FSPL = 10\log_{10}\left(\frac{P_T}{P_R}\right) \qquad 2.1$$

$$\text{FSPL} = -10\ \log_{10} G_T - 10\ \log_{10} \text{G}_\text{R} + 20\ \log_{10} f + 20\log_{10} d + \text{K}$$

Where $k = 20\log_{10}(\frac{4\pi}{3\times 10^8}) = -147.56$, and FSPL free space propagation loss

2.6.2 Atmosphere Losses

As contrast to microwave wireless networks with lower carrier frequencies, millimeter wave wireless communications suffer from a larger propagation path loss caused by gas molecules in the Earth's atmosphere. Atmospheric loss, also known as gaseous attenuation, is caused by molecules absorbing a portion of the energy propagating waves and vibrating proportionally to the carrier frequency[1]. Oxygen (O2) and water vapor (H2O) gas cause severe attenuations in millimeter waves [24, 33]. Other inter-related factors include temperature, altitude, pressure, and, most importantly, operating carrier frequency, which defines the intensity of gaseous absorption [1].

Both dry air (oxygen) and water vapor have effects on the transmission of high frequency bands, as seen in figure 2.3 [21], a simplified and combined conclusion of oxygen and water vapor attenuation on the millimeter wave. The O2 absorption peaks are found at 60 GHz with more than 10 dB/km loss and about 120 GHz with 1.4 dB/km loss, respectively, by using sea level with maximum air density as the worst case for atmospheric attenuation.

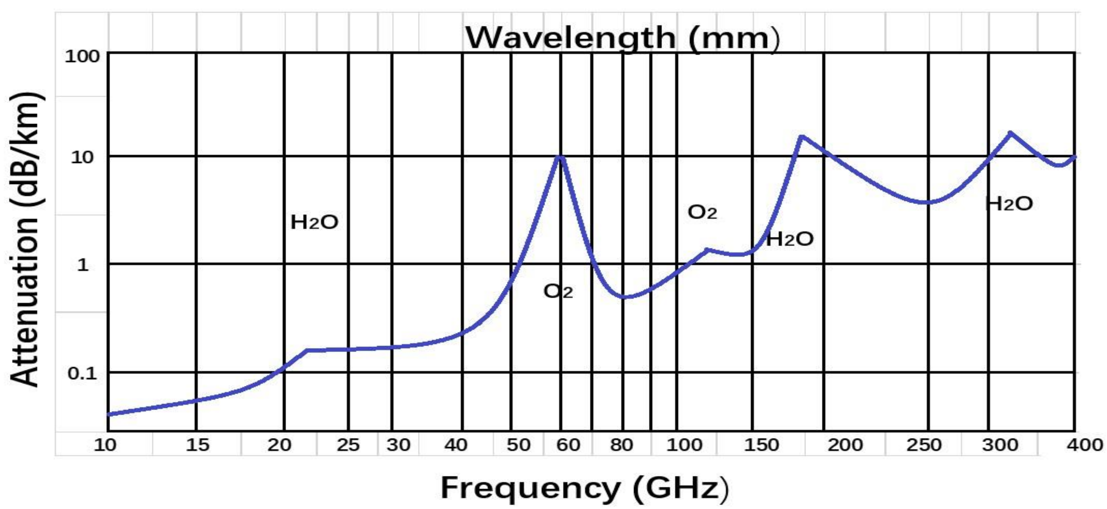

Figure 2.3: Specific attenuation of O2, H2O and rain at sea level[21]

Figure 2.3 show that the loss of H2O molecules occurs at frequencies 23GHz and 183GHz, loss of 0.18dB/km and 28.35dB/km respectively. The three mains attenuation at 60GHz, 183GHz and approximately 323GHz with maximum attenuation of 38.6dB/km at the later, and two smaller maximum at 23GHz and around 120GHz, are collectively refer to atmosphere attenuation resonant [33]. Since H2O and O2 resonant bands do not match it, air losses occur to have a minor influence on millimeter wave transmissions, particularly over short distances.

2.6.3 Rain Attenuation

In millimeter waves, rain attenuation and losses due to rain are relevant. At millimeter wave frequencies, raindrops are roughly the same size as radio wavelengths. As a result, raindrops easily block millimeter wave signals, causing the signal's energy to be scattered and its strength to be lost [33]. According to some studies, rain attenuation is proportional to rainfall rate. The rain loss of the signal increases with heavier rain falls, according to reports. The data from the 70 GHz experimental measurements indicate that in a situation of light rain at 1 mm per hour, the signal loss is about 0.9 dB/km, whereas a larger rain rate of 50 mm per hour results in an exponential rise to 18.4 dB/km.

Furthermore, the effect of rain varies depending on the frequency bands of millimeter waves. Higher frequencies suffer greater rain losses at the same rain rate. Rain attenuation in millimeter wave and designated sub-100 GHz bands for 5G is more problematic than rain attenuation in conventional microwave networks. The path loss due to rain attenuation is not significant with shorter range communication in the order of 200 m. In indoor scenarios and dense urban areas with cell sizes of less than 200 meters, higher frequency millimeter waves are used.

2.6.4 Material Penetration

Mmwave frequency are also sensitive to penetration loss, and cannot penetrate various solid materials doors, window, walls, and room furniture ,when compared to microwave [1, 6]. The table 2.2 indicate that outdoor and indoor measurement results by Zhao H. et al [6].

Table 2.2: Based on the measurements various material penetration loss in dB/cm[6]

Environments	Materials	Thickness(Cm)	Penetration Loss(Db)
Outdoor	Tinted glass	3.8	40.1
	brick	185.4	28.3
indoor	clear glass	< 1.3	3.9
	Tinted glass	< 1.3	24.5
	clear glass	< 1.3	3.6
	wall	38.1	6.8

2.6.5 Blockage Intensity

One of the unique elements of mmWave cellular communication is the propagation environment. Because mmWave signals are blocked by certain materials, such as concrete walls, resulting in significant penetration loss, it is more sensitive to network blockages than microwave frequency bands. Blockages cause significant differences in the loss characteristics of LOS and NLOS paths [34]. According to research, mmWave is sensitive to blockages for three reasons: first, high penetration losses while traveling through many common materials, second, mmWave frequencies do not diffract well in terrestrial environments, and third, because of requirements of directionality.

Stochastic physical channel model with an intensity of Λ blockings/m^2 was used to generate the number of blockings. Just for simplicity, the blockings are assumed to be made up of lines, with the center of each blocking being uniformly selected in the cellular network area figure 2.4 shown. The angle of each blocking line is then uniformly chosen in the interval $(0, 2\pi)$.

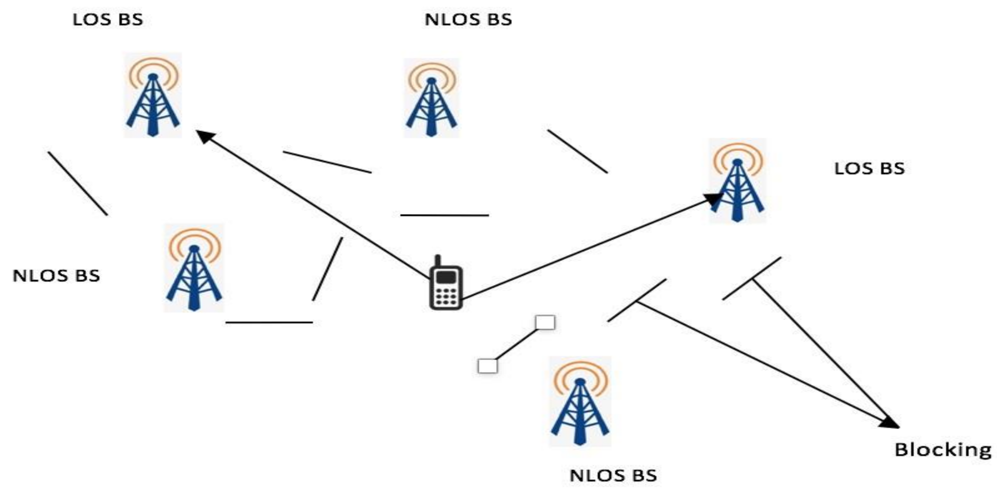

Figure 2.4: Blockage with system model for millimeter wireless communication[34]

2.7 Propagation in Different Environments

Most of the time environment contain obstruction between the receiver and transmitter which are: tree, walls, person, building etc. the practical area free space model is varied. Determine signal strength by different study in different environments [35].

2.7.1 Flat Terrain

The directed signal follows free space model, whereas reflected signal equal to the multiply of reflection index and cosine of angle of ground reflection shown in figure 2.5.

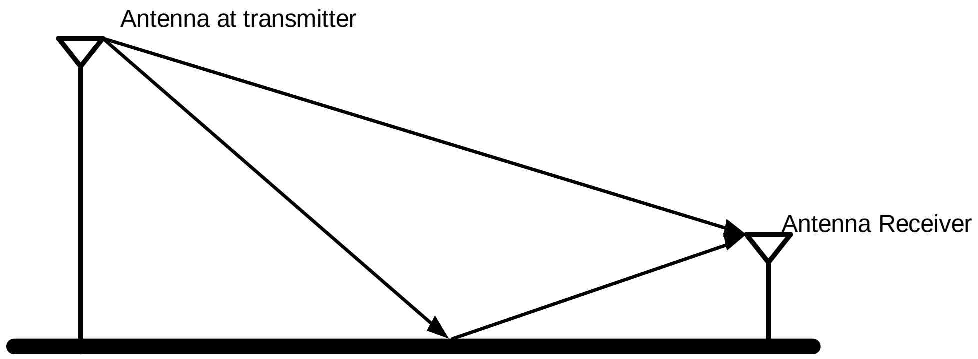

Figure 2.5: Flat terrain propagation

2.7.2 Rough Terrain

There are different sides diffuse scattering or reflection in rough terrain, which is depends on the rough surface area that are equivalent to the incident signal wavelength and incident angle. The surface can be considered smooth from certain incident angles, as shown in figure 2.6, principal called the Rayleigh criteria is commonly used.

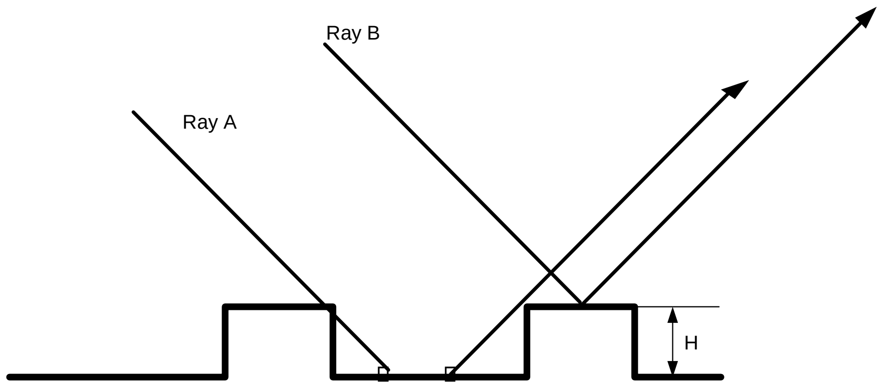

Figure 2.6: Irregular surface Rayleigh criterion

Signal path differ between two ray A and B written as.

$$\Delta d = 2Hsin\theta \qquad 2.2$$

And also angle difference

$$\Delta\theta = \frac{4\pi H}{\lambda}\sin\theta \qquad 2.3$$

In practical radio propagation the value of θ is quite small and σ standard deviation replace H height so equation 2.3 written as:

$$K \cong \frac{4\pi\sigma\theta}{\lambda} \qquad 2.4$$

Where k>10 the surface is diffused reflector highly so signal is reflected is significantly small that it can ignored ,if k < 0.1, smooth surface it considered.

2.8 Multipath Phenomena

Multipath is one of the most significant features of cellular network. As seen in figure 2.7, multiple radio signals from at least two different directions enter the transmitting antenna in a short period of time for the same transmitted signal. They are more likely to arrive with varying magnitudes and phases when they come from different directions. As a result, the collected signals at the receiving antenna's resultant waveform is a summation of all vectoral signal. It can add to or subtract from the final signal depending on the magnitude and phase of each signal. As a consequence, the signal generated may be either strong or faded. Short term fading and long-term fading are the two types of fading. Long term fading is the movement of receiver over distance and cause to changing in the signal magnitude. While short term transmitted signal replicas caused by close scatterers arrive to receiver antenna with various time delays magnitude and phase.

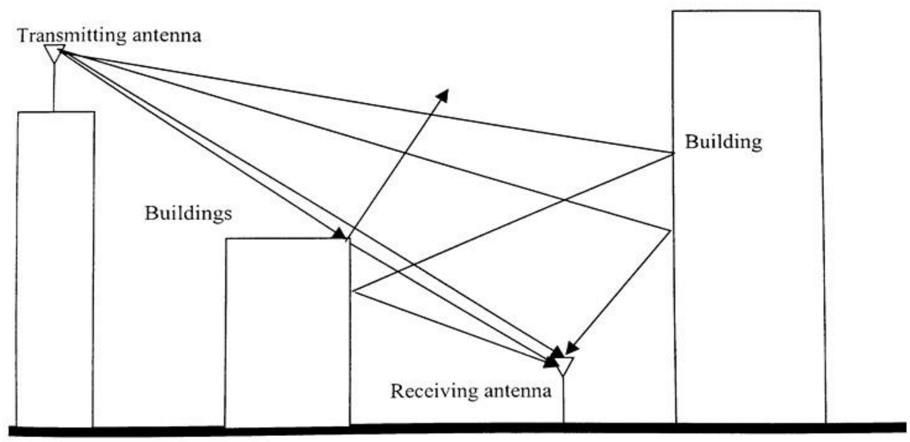

Figure 2.7: Different LOS/NLOS via Propagation

CHAPTER THREE

3. MATERIALS AND METHODS

3.1 Millimeter Wave and Microwave Difference

High-frequency radio waves have different propagation characteristics compared to microwaves due to the increase in frequency. Millimeter waves cannot diffract and penetrate effectively through obstructions, for example, buildings, the human body, and cars. This consequences in lower diffracting of the high path loss and multipath components (MPC), emphasis on numerous channel characteristics in the mmWave bands in the following subsections.

3.2 Parameters and Statistics

There are numerous criteria used to describe the channel properties in practice. Most of them concentrate on arithmetical analysis. The power delay profile, the root mean square (RMS), and the average delay spread are the most commonly used parameters. Received signal strength, fading, and path loss are the most often used parameters when determining channel path loss. Angle of arrival (AoA), angle of departure (AoD), and their RMS angular spread are usually used to measure angular parameters. These parameters are vital because they provide the essential evidence for channel modeling and device design.

3.2.1 Power Delay Profile (PDP)

Over a multipath channel, they describe the received signal strength as a function of the propagation delay wave. It can be measured empirically and used to determine channel parameters such as path loss, angular parameters (i.e. angle of arrival, angle of departure, and RMS angular spread), delay spread, and signal frequency. The power delay profile, which runs from the original signal that reaches the receiver to the last signal whose power level over specific thresholds, can be used to predict the average power of a multipath channel.

3.2.2 Average, RMS Delay Spread and Excess Delay Spread

These three parameters are primarily used to describe the channel time properties. The primary key to defining them is the power delay profile analysis. Where the initial moment of the power delay profile is identical to the average excess delay ($\bar{\tau}$).

$$\bar{\tau} = \frac{\sum_k P(\tau_k)\tau_k}{\sum_k P(\tau_k)} \qquad 3.1$$

The square root of the second central moment of the power delay profile is equal to the RMS delay spread (σ_τ) and is given by:

$$\sigma_\tau = \sqrt{\overline{\tau^2} - (\bar{\tau})^2} \qquad 3.2$$

Where

$$\overline{\tau^2} = \frac{\sum_k P(\tau_k)\tau_k^2}{\sum_k P(\tau_k)} \qquad 3.3$$

Where τ = 0, the delays are measured relative to this point.

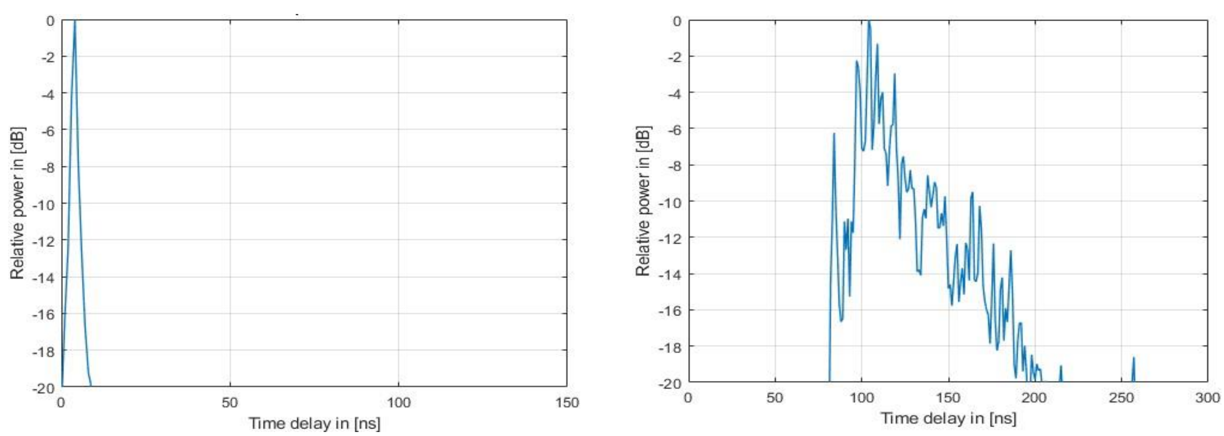

(a) (B)

Figure 3.1: Delay spread from an impulse signal (a) transmitted signal (b) received signals [36]

The delay spread can be seen in Figure 3.1. Due to the multipath effect, where the arrival time to the receiver varies from one signal to another depending on their path distance, the transmitted signal is shown in figure 3.1 (a) and the replicated components at the receiver are shown in figure 3.1 (b). The shortest propagation path is defined by the first peak.

3.2.3 Doppler Spread

The channel time nature is defined by the delay spread parameters. However, include details on the channel time variant nature caused by the relative motion between the transmitter and receiver or the movement of objects in the channel. Because of the movement, the propagation path lengths can change, either due to the change in receiver location or due to the Doppler Effect caused by the movement. In the propagation direction, the phase change rate appears as a Doppler frequency shift.

3.2.4 Signal Strength and Path Loss

The majority of the models presented were for outdoor scenarios, and all path loss measurements in this analysis were done in both outdoor and indoor environments. Path loss estimation requires a different method for indoor and outdoor propagation calculations. As a result, three recommended path loss models for outdoor to indoor measurements were chosen: the close-in (CI), close-in with frequency weighted path loss exponent, and the floating-intercept (FI) path loss models. The CI path loss model is given in equation 3.4.

$$PL^{CI}(f,d)[dB] = FSPL(f,d_0) + 10nlo\,g_{10}\left(\frac{d}{d_0}\right) + X_\sigma \quad for\ d \geq d_0 \qquad 3.4$$

Where n is the path loss exponent,d_0 =1m for the mmWave and X_σ is a zero mean Gaussian random variable with standard deviation σ in dB [36].

The second path loss model is close-in with frequency weighted path loss exponent, to calculate average path loss ended distance, and return to the single parameters CI model when $b = 0$ for multi frequency or a single frequency $f = f_0$ is modeled, two parameters are required [37]

$$PL^{CIF}(f,d)[dB] = 32.4 + 20\log_{10} f_c + 10n(1 + blo\,g_{10}\left(\frac{f - f_0}{f_0}\right) + X\sigma^{CIF} \qquad 3.5$$

Where n is the distance dependent path loss, b is an optimization parameters that refer to the linear dependence of path loss around weighted average of frequencies f_0 (in GHz), from the data recycled to optimize the model.

Third floating intercept (FI) or Alpha-beta-gamma (ABG) path loss models, is given in equation 3.6. Three parameters are needs the power of transmitted is not considered.

$$PL(d)[dB] = \alpha + 10\beta\log_{10}(d) + X_\sigma \qquad 3.6$$

Where α is the floating-intercept in dB, β is the slope of the fitting line and X_σ the same as in the CI model is a zero mean Gaussian random variable with standard deviation σ in dB.

3.2.5 Angle of Arrival or Departure

The power mean pointing angle ($\bar{\theta}$) of a certain denoted by AoA or AoD which determine from equation 3.7.

$$\bar{\theta} = \frac{\sum_k P(\theta_k)\theta_k}{\sum_k P(\theta_k)} \quad 3.7$$

Where k is a pointing angle index θ_k(degrees) of each angle above a pre-defined threshold level within a lobe and $P(\theta_k)$ is the received power (mW) at θ_k [38].

3.2.6 RMS Angular Spread

The RMS elevation or azimuth elevation angular spread is described as the second moment of the power angular profile in azimuth or elevation and indicates the standard deviation of power-weighted of the azimuth or elevation directions of arrival or departure and is calculated using equation 3.8.

$$\sigma_\theta = \sqrt{\overline{\theta}^2 - (\bar{\theta})^2} \quad 3.8$$

$$\overline{\theta}^2 = \frac{\sum_k P(\theta_k)\theta_k^2}{\sum_k P(\theta_k)} \quad 3.9$$

Where k a lobe and P(θ_k) is the received power (mW) at θ_k [38].

3.2.7 Nakagami Fading

Rayleigh and Rican fading models have been widely used to simulate small scale fading environments over decades. States that Rayleigh fading falls short in describing long distance fading effects with sufficient accuracy. Nakagami observed this fact and then formulated a parametric gamma function to describe his large-scale experiments on rapid fading in high frequency long-distance propagation. Although empirical, the formula is rather elegant and has proven useful. The form of the Nakagami-m distribution is given below.

$$p(r) = \frac{2}{\Gamma(m)}\left(\frac{m}{\Omega_p}\right)^m r^{2m-1} \exp\left(-\frac{mr^2}{\Omega_p}\right) \qquad 3.10$$

Where $m \geq \frac{1}{2}$ is fading figure, Ω_p is instantaneous power, and r is gamma functions

3.3 Millimeter Wave Channel Model

Physical channel models and analytical-based channel models are the two types of channel models that are classified. An analytical channel model is designed on the basis of mathematical analysis, while a physical channel model is designed on the basis of propagating signal characteristics between the transmitter and receiver antenna arrays [1]. In this thesis, we used a stochastic physical channel model that is based on comprehensive measurements and is probabilistic for describing the characteristics of multipath components' spatial and temporal behavior (MPCs). The computational complexity of the deterministic model is higher. Another advantage of stochastic channel models is that they have lower computational complexity and take less time to compute, making them suitable for simulation and system design [1].

Table 3.1: Modeling of channel for millimeter wave by several organization [1].

Technologies	Frequency(GHz)	year	Channel Model	Description
5G	28 GHz, 38 GHz, and 73 GHz	Since 2015	5GCM	There has been a lot of study mmwave channel designing, mostly at the frequencies of 28 GHz, 38 GHz, and 73 GHz. First, a narrowband proposition, followed by a range of wideband channels[39].
5G	up to 100 GHz	2012	METIS	5GPPP millimeter wave channel model for mobile systems. The model is based on the WINNER II and WINNER + channel modeling techniques[19].
5G	up to 100 GHz	2017	3GPP	The new 3GPP series 38.900 channel models which is an extension of 3GPP TR 36.873, commonly used for sub-6 GHz bands. The current model supports azimuthal and elevation characteristics of the channel. Various scenarios as well as sub-100 GHz bands are supported[40].
5G	6-100 GHz	2015	mm MAGIC	The European Commission has launched an investigation 5G use of mmWaves. The mmMAGIC using a vast volume of data from 22 channel measurement campaigns, as well as intensive modeling and validation efforts[41].

3.4 Design Consideration

3.4.1 Frequency Range

For 5G cellular communication, the millimeter wave (mmWave) spectrum is a strong candidate. The practical range for mmWave is from 500 MHz to 100 GHz. For 5G, very high frequencies, using higher frequencies contributes to very high losses in propagation. In general, if the operating frequency is increased, the radio signal dies out at a shorter distance for the following reasons [42, 43].

- Typically, at lower frequencies, as the radio wave penetrates through obstacles, the objects absorb less energy. Thus, at greater frequencies, the penetration loss is typically higher.
- Since this lower frequency allows for a greater angle of diffraction, the radio wave can bend around obstacles more easily. As a result, the radio signal will be able to reach more people and the coverage area will be minimized.
- Higher frequencies absorb higher energy when the radio wave is reflected by objects. As a result, the reflected wave has less power at a higher frequency.

5G will not provide almost as much coverage as 4G or 3G. It will be difficult for the 5G signal to penetrate solid objects such as walls, windows, and even trees. 5G packets are deployed in heavily trafficked areas [44].

3.4.2 Data Rate Demand

The demand and number of wireless users for an individual user's data rate are increasing exponentially with time. The rise in the number of wireless devices is highly affected by the advent of internet of things (IoT) devices. The increase in the demand for individual data rates is seriously influenced by the introduction of high-quality online games and video apps. Thus, the overall demand for data rates is rising dramatically.

3.4.3 High Frequency Use

The increase in data rate demand causes the requirement for bandwidth to increase by bounds and leaps. In order to meet this need, at the lower frequency ranges are occupied, wireless communication gradually uses higher frequencies. While mobile networks are well-defined for frequencies under 6 GHz so far, 5G cellular systems of the next generation will cover frequencies from around 500 MHz to around 100 GHz. The use of higher frequencies significantly increases the loss of propagation, which makes the problem of wireless coverage much more difficult and complex.

The user experience of the data rate depends on the signal-to-interference plus noise ratio (SINR) received by the user.

$$\mathrm{SINR} = \frac{P_R}{N + I} \qquad 3.11$$

Where P_R represents the desired signal power received, I represents the interference power received from other sources, and N is the noise power received.

Technically, the experience of the data rate depends directly on the SINR, because higher SINR allows higher modulation and coding scheme (MCS) levels to be used and reduces the retransmission of erroneous packets. The user data rate in bits/sec also depends on the used frequency range, B_W, the technology used in the data transfer, and the allowed or target Bit Error Rate (BER). The BER represents the number of bits in error divided by the total number of transferred bits. The user data rate in bits/sec is specified by:

$$\mathrm{R} = \mathrm{B_W} * \log_2(1 + \alpha\mathrm{SINR}) \qquad 3.12$$

Where α is constant for target BER, and defined by $\alpha = 1.5/\log_e(5.\mathrm{BER})$ the target BER is commonly set to 10^{-6} [45].

The user device receives the desired signal from the neighboring BS (in LOS or NLOS), but it also receives interference from the base station. It is assumed that P_R is the power obtained from the BS, I is the interference power received from the base stations, N_O is the spectral intensity of white noise power, and B_W refers to the bandwidth used. Then according to equation 3.10. The signal-to-interference plus noise ratio (SINR) for the UE can be expressed by;

$$\mathrm{SINR} = \frac{\mathrm{P_R}}{\mathrm{N_O} * \mathrm{Bw} + \mathrm{I_{BS}}} \qquad 3.13$$

The power obtained from a transmitter can be calculated as PL. G and PT are transmit power and the channel gain is represented by G. The relationship between channel gain and PL path losses can be seen as [45], ignoring the small-scale fading and shadowing effects.

$$G = 10^{-\frac{PL}{10}} \quad 3.14$$

To evaluate G, the Path Loss PL needs to be measured. Among the path loss models, which support frequency bands up to 100 GHz, has been used for research due to the expectation of 5G systems. For outdoor-to-indoor conditions, the ABG and CI path loss models. As the signal enters from the base station inside the building, due to outdoor-to-indoor building penetration loss [9], the total path loss will then be approximately.

$$PL_{total} = PL_{outdoor} + BPL \quad 3.15$$

Ignoring the loss due to the receiver's position away from the building's exterior wall. BPL properties for frequencies up to 100 GHz have been investigated. They used an approach based on extensive measurements and showed that the efficient BPL in dB fits into the relationship below.

$$BPL = 10\log_{10}(A + Bf^2) \quad 3.16$$

Here, depending on the building's condition, f is frequency in GHz and A and B are constants. When the building has low BPL [46], they set A = 5 and B = 0.03 and they set A = 10 and B = 5 when the building has high BPL.

3.4.4 LOS Probability Model

This model is required to determine whether the base station is located directed LOS from user equipment (UE) or is NLOS. The LOS probability is frequency-independent and is characterized as a function of the receiver and transmitter, which can be altered by environmental design.

The 3GPP and 5GCM channel models are the most commonly referenced in studies among the current channel models developed by various groups. NYUSIM (5GCM) is used for all simulations in this thesis since it has been shown in [47] to be more accurate than 3GPP. Focusing on Urban Microcell (UMi) and Urban Macrocell (UMa) scenarios with different frequency bands in 5GCM [9].

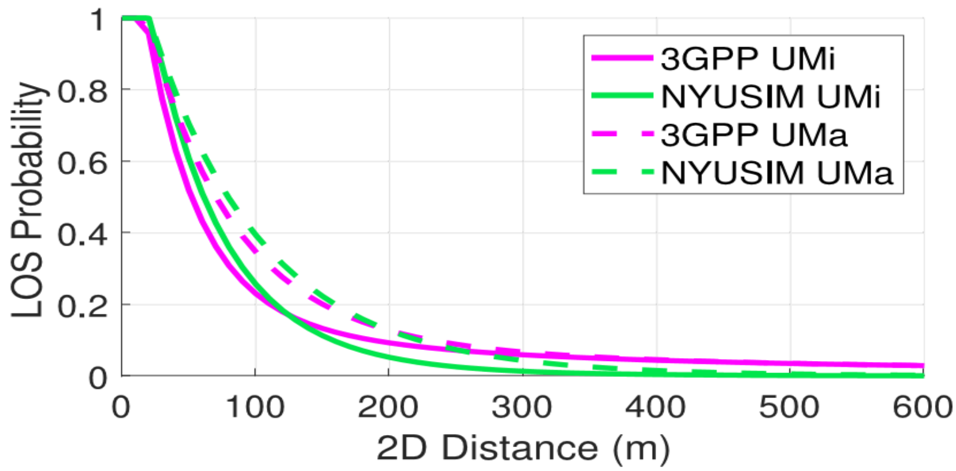

Figure 3.2: LOS probability models comparison in NYUSIM and 3GPP channel model[48]

NYUSIM predicts a greater probability of LOS compared to 3GPP for distances smaller than about 120 m (for UMi) or 160 m (for UMa) for T-R separations. The simulated LOS probability is 9.1 percent and 17.2 percent using the 3GPP and NYUSIM models, respectively, shown in figure 3.2, through 500 random selected user location simulation runs for the UMi street canyon scenario over distances from 10 m to about 300 m (where cell size was based on the condition that 95 percent of the area within a cell has an SNR equivalent to 5dB.

The difference in the probability of LOS affects spectral efficiency, as LOS facilitates stronger mmWave propagation (i.e. greater SNR) compared to NLOS due to more severe loss of diffraction at mmWave frequencies than at sub-6 GHz.

3.4.4.1 UMi LOS Probability Model

The UMi scenario is planned for highly populated areas of up to 200 m inter-site distances (ISDs) and the height of the base station is below rooftops. A number of organizations developed UMi probability models, as shown in Table 3.2. 5GCM used throughout this thesis.

Table 3.2: 5GCM in UMi and UMa scenarios LOS probability model[49]

UMi	$\frac{d_1}{d_2}$ model: $PLOS(d_{2D}) = \min\left(\frac{d_1}{d_{2D}}, 1\right)(1 - \exp(-d_{2D} = d_2)) + \exp(d_{2D} = d_2)$ $NYU(squared)\ model\ :PLOS(d_{2D}) = \left(\min\left(\frac{d_1}{d_{2D}}, 1\right)\left(1 - \exp\left(\frac{d_{2D}}{d_2}\right)\right) + \exp(-d_{2D} = d_2)\right)^2$	$d1/d2\ model$: $d1 = 20\ m, d2 = 39\ m$ $NYU\ (squared)\ model: d1 = 22\ m, d2 = 100\ m$
UMa	$d1/d2\ model$: $P_{LOS} = (min\ (d_1 = d_{2D}, 1)\ (1 - exp(-d_{2D}/d_2) + exp(d_{2D}/d_2))\ (1 + C\ (d_{2D}, h_{UE})$ NYU (squared) model: $P_{\ LOS} = ((\min(d_1/d_{2D}, 1)\ (1 - \exp(-d_{2D}/d_2)) + \exp(-d_{2D}/d_2)\ (1 + C\ (d_{2D}, h_{UE})))2$	$d1/d2\ model: d1 = 20\ m, d2 = 66\ m$ $NYU\ (squared)\ model: d1 = 20\ m, d2 = 160\ m$

3.4.4.2 UMa LOS Probability Model

The UE height in the Urban Macrocell (UMa) scenario is 1.5 m, and BSs are typically designed at 25-30 m above rooftop heights, with up to 500 m ISD. Table 3.4 [49] also contains the UMa LOS probabilities, similar to the UMi LOS probabilities with the exception of the d2 and d1 values.

3.4.5 Large Scale Path Loss Model

Basic three kinds of large scale path loss models: close-in, close-in frequency weighted and ABG or FI path loss models are used for estimating signal strength over a distance. The CI path loss of different frequencies has more consistency and less complexity [50], but the ABG path loss model is more accurate at reaching floating points.

3.4.5.1 UMi Large Scale Path Loss Model

As shown in Table 3.3, the UMi scenario is commonly referred to as an open square or street canyon. The CI and ABG were chosen by the 5GCM for modeling the UMi NLOS path loss. Only the PLE, a single parameter, is determined in the CI path loss model in order to mitigate the model error of mean loss over distance through optimization. To mitigate model errors, three parameters, i.e. α, β and γ also, must be enhanced in the ABG model.

Table 3.3: UMi scenarios omnidirectional path loss model [49]

	PL[dB], f_c in GHz and d_{3D} in meters	Shadow fading std [dB]	Application range and parameters
5GCM[5]			
5GCM UMi-street canyon LOS	CI model with 1m reference distance $PL = 32.4 + 21\log_{10}(d_{3D}) + 20\log_{10}(f_c)$	$\sigma_{SF} = 3.76$	$6 < f_c < 100GHz$
5GCM UMi-street canyon NLOS	CI model with 1m reference distance $PL = 32.4 + 31.7\log_{10}(d_{3D}) + 20\log_{10}(f_c)$ ABG model $PL = 22.4 + 35.3\log_{10}(d_{3D}) + 21.3\log_{10}(f_c)$	$\sigma_{SF} = 8.09$ $\sigma_{SF} = 7.82$	$6 < f_c < 100GHz$
5GCM UMi-Open square LOS	CI model with 1m reference distance $PL = 32.4 + 18.5\log_{10}(d_{3D}) + 20\log_{10}(f_c)$	$\sigma_{SF} = 4.2$	$6 < f_c < 100GHz$
5GCM UMi-street canyon NLOS	CI model with 1m reference distance $PL = 32.4 + 28.9\log_{10}(d_{3D}) + 20\log_{10}(f_c)$ ABG model $PL = 3.66 + 41.4\log_{10}(d_{3D}) + 24.3\log_{10}(f_c)$	$\sigma_{SF} = 7.1$ $\sigma_{SF} = 7.0$	$6 < f_c < 100GHz$
3GPP TR 38.901 V14.0.0			
3GPP UMi-street canyon LOS	$PL_{UMi-LOS} = \begin{cases} PL1, & 10m < d_{2D} < d'_{BP} \\ PL2, & d'_{BP} < d_{2D} < 5km \end{cases}$ $PL_1 = 32.4 + 21\log_{10}(d_{3D}) + 20\log_{10}(f_c)$	$\sigma_{SF} = 4.0$	$0.5 \leq f_c \leq 100GHz$ $1.5 \leq h_{UE} \leq 22.5m$ $h_{BS} = 10m$

	$PL_2 = 32.4 + 40\log_{10}(d_{3D}) + 20\log_{10}(f_c) - 9.5\log_{10}(d'_{BP})^2 + (h_{BS} - h_{UE})^2$ Where d'_{BP} is specified in equation(8)		
3GPP UMi-street canyon NLOS	$PL = \max(PL_{UMi-LOS}(d_{3D}), (PL_{UMi-NLOS}($ $PL_{UMi-NLOS} = 22.4 + 35.3\log_{10}(d_{3D}) + 21.3\log_{10}(f_c) - 0.3(h_{UE} - 1.5)$ Option: CI model with 1m reference distance $PL = 32.4 + 31.9\log_{10}(d_{3D}) + 20\log_{10}(f_{c)}$	$\sigma_{SF} = 7.82$ $\sigma_{SF} = 8.2$	$0.5 < f_c < 100GHz$ 10m<$d_{3D} < 5000m$ $1.5m \leq h_{UE} \leq 22.5m$ $h_{BS} = 10m$
METIS			
METIS UMi-street canyon LOS	$PL_{UMi-LOS} = \begin{cases} PL1, & 10m < d_{2D} < d_{BP} \\ PL2, & d_{BP} < d_{2D} < 500m \end{cases}$ $PL_1 = 28 + 22\log_{10}(d_{3D}) + 20\log_{10}(f_c) + PL_0$ $PL_2 = 7.8 + 40\log_{10}(d_{3D}) + 2\log_{10}(f_c) - 18\log_{10}(h_{BS} * h_{UE}) + PL_1(d_{BP})$ Where d_{BP} and PL_0 is specified in equation(9) and (10)	$\sigma_{SF} = 3.1$	$0.8 \leq f_c \leq 60GHz$

METIS UMi-street canyon NLOS	$PL = \max(PL_{UMi-LOS}(d_{3D}), (PL_{UMi-NLOS}($ $PL_{UMi-NLOS} = 22.4 + 35.3\log_{10}(d_{3D}) + 21.3\log_{10}(f_c) - 0.3(h_{UE})$	$\sigma_{SF} = 4.0$	$0.45 \leq f_c \leq 6GHz$ 10m< $d_{3D} < 2000m$ $1.5m \leq h_{UE} \leq 22.5m,$ $h_{BS} = 10m$
mm MAGIC			
mm MAGIC UMi-street canyon LOS	$PL = 32.+19.2\ \log_{10}(d_{3D}) + 20.8\log_{10}(f_{c)}$	$\sigma_{SF} = 2.0$	$6 < f_c < 100GHz$
mm MAGIC UMi-street canyon NLOS	$PL = 31.0 + 45.0\ \log_{10}(d_{3D}) + 20.0\log_{10}(f_{c)}$	$\sigma_{SF} = 7.82$	$6 < f_c < 100GHz$
Note :PL is path loss, d_{3D} *is the* 3D T-R *Eucuidean distance*			

3.4.5.2 UMa Large Scale Path Loss Model

Close-in (CI), CI with frequency weighted (CIF), and ABG are the three UMa path loss models that are included in the 5GCM [9]. In the NLOS scenario, the CI and ABG are used, while in the UMi LOS scenario, the CI is used. The path loss models of 5GCM and other organizations are described in below table 3.5 [49].

Table 3.4: UMa Scenarios Omnidirectional Path Loss Model [49]

	PL[dB], f_c in GHz and d_{3D} in meters	Shadow fading std [dB]	Application range and parameters
5GCM[5]			
5GCM UMa- LOS	CI model with 1m reference distance $PL = 32.4 + 20\log_{10}(d_{3D}) + 20\log_{10}(f_c)$	$\sigma_{SF} = 4.1$	$6 < f_c < 100GHz$
5GCM UMa- NLOS	CI model with 1m reference distance $PL = 32.4 + 30\log_{10}(d_{3D}) + 20\log_{10}(f_c)$ ABG model $PL = 19.2 + 34\log_{10}(d_{3D}) + 23\log_{10}(f_c)$	$\sigma_{SF} = 6.8$ $\sigma_{SF} = 6.5$	$6 < f_c < 100GHz$
3GPP TR 38.901 V14.0.0			
3GPP UMa- LOS	$PL_{UMi-LOS} = \begin{cases} PL1, & 10m < d_{2D} < d'_{BP} \\ PL2, & d'_{BP} < d_{2D} < 5km \end{cases}$ $PL_1 = 28 + 22\log_{10}(d_{3D}) + 20\log_{10}(f_c)$ $PL_2 = 28 + 40\log_{10}(d_{3D}) + 20\log_{10}(f_c) - 9\log_{10}(d'_{BP})^2 + (h_{BS} - h_{UE})^2$ Where $d'_{BP} = h'_{BS}h'_{UE} \times f_c \times 10^9/c$ is specified in equation(8)	$\sigma_{SF} = 4.0$	$0.5 \leq f_c \leq 100GHz$ $1.5 \leq h_{UE} \leq 22.5m$ $h_{BS} = 25m$

3GPP UMa-NLOS	$PL = \max(PL_{UMa-LOS}(d_{3D}), (PL_{UMa-NLOS}(d_{3D}$ $PL_{UMi-NLOS} = 13.54 + 39.08\log_{10}(d_{3D}) + 20\log_{10}(f_c) - 0.6(h_{UE} - 1.5)$ Option: CI model with 1m reference distance $PL = 32.4 + 30\log_{10}(d_{3D}) + 20\log_{10}(f_{c)}$	$\sigma_{SF} = 6.0$ $\sigma_{SF} = 7.8$	$0.5 < f_c < 100GHz$ 10m<$d_{3D} < 5000m$ $1.5m \leq h_{UE} \leq 22.5m$ $h_{BS} = 25m$
METIS			
METIS UMa- LOS	$PL_{UMa-LOS} = \begin{cases} PL1, & 10m < d_{2D} < d_{BP} \\ PL2, & d_{BP} < d_{2D} < 500m \end{cases}$ $PL_1 = 28 + 22\log_{10}(d_{3D}) + 20\log_{10}(f_c) + PL_0$ $PL_2 = 28 + 40\log_{10}(d_{3D}) + 20\log_{10}(f_c) - 9\log_{10}(d'_{BP})^2 + (h_{BS} - h_{UE})^2$ Where $d'_{BP} = 4(h_{BS} - 1)(h_{UE} - 1) \times 10^9/c$	$\sigma_{SF} = 4.0$	$0.45 < f_c < 6GHz$ 10m<$d_{3D} < 2000m$ $1.5m \leq h_{UE} \leq 22.5m$ $h_{BS} = 25m$
METIS UMa-NLOS	$PL = \max(PL_{UMa-LOS}(d_{3D}), (PL_{UMa-NLOS}(d_{3D}$ $PL_{UMi-NLOS} = 161.94 + 7.1\log_{10} w + 7.5\log_{10} h - (24.37 - 3.7\left(\frac{h}{h_{BS}}\right)^2)\log_{10}(h_{BS}) + (43.42 - 3.1\log_{10}(h_{BS}))(\log_{10}(d_{3D}) - 3) + 20\log_{10}(f_c) - 0.6(h_{UE})$	$\sigma_{SF} = 6.0$	$0.45 < f_c < 6GHz$ 10m<$d_{3D} < 2000m$ $1.5m \leq h_{UE} \leq 22.5m$ $h_{BS} = 25m, w = 20m, h = 20$

3.4.6 Millimeter Wave Link Budget

The received signal level (RxSL) at the receiver is determined by calculating the overall gain and loss in the system (UE). After that, comparing the receiver sensitivity (RxS) to the received signal level is to determine whether the channel failed or passed the design as shown in figure 3.3. If the received signal frequency (RxSL) is greater than the reception sensitivity (RxS), the channel status is "Pass," otherwise it is "Fail." The 5G link budget received signal level (RxSL) is calculated using the following flow chart.

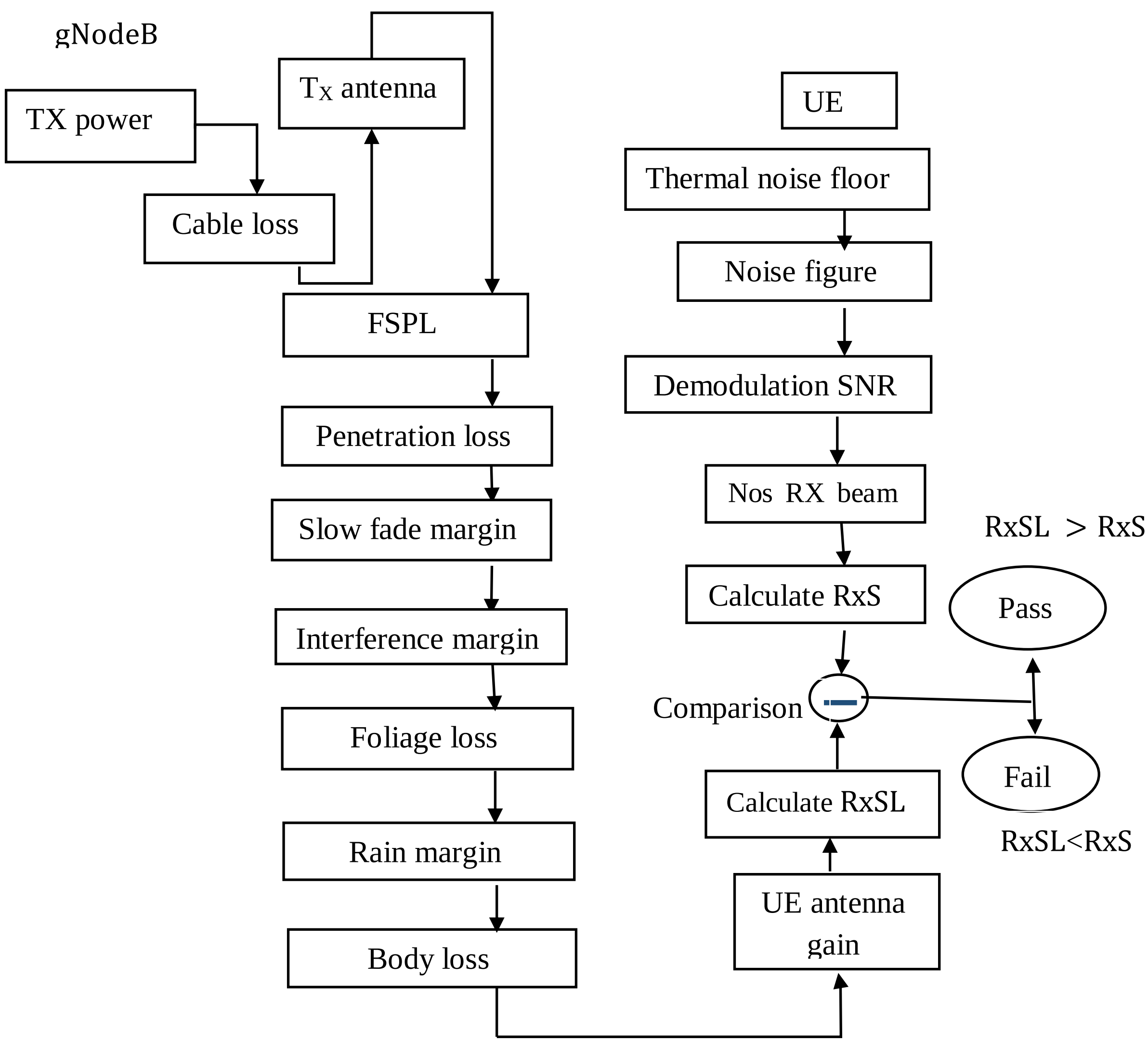

Figure 3.3: Block diagram of overall gain and loss

$$\text{Received Signal Level at receiver (dBm)}$$
$$= \text{gNodeB Tx power(dBm)} - 10\log_{10}(\text{sub carrier quantity})$$
$$+ \text{gNodeB antenna gain(dBi)} - \text{gNodeB cable loss(dB)} - \text{body block loss}$$
$$- \text{slow fading margin} - \text{foliage loss} - \text{rain margin} - \text{interference margin}$$
$$- \text{atmospher loss} - \text{penetration loss} + \text{UT antenna gain}$$
$$- \text{thermal noise figure} - \text{UT noise figur} - 16$$
$$- \text{QAM SINR (dB)} \qquad 3.17$$

To determine the path loss, we need to use a suitable propagation model for the 5G 5GCM channel model. The frequency bands of 0.5–100 GHz are applicable for UMi, and UMa in the 5GCM model.

Table 3.5: 5G mm wave link budget parameters for outdoor to indoor at 28 GHz

	Uplink calculations	Downlink calculations
Parameters	Values	values
Channel Bandwidth (GHz)	800	800
TX antenna Gain (dBi) [51]	27	27
Subcarrier quantity [52]	1584	1584
Resource block [52]	132	132
TX power (dBm) [51]	30	30
Cable loss (dB) [52]	2	2
EIRP(dB)	57	57
RX antenna Gain (dBi)[52]	21	21
RX Noise figure (dB) [51]	7	7
Thermal Noise (dBm/Hz) [52]	-154.93	-154.93
atmospheric attenuation (dB/Km) [52]	0.06	0.06
Rain attenuation (dB/Km) [51]	3.45	3.45
Foliage losses (dB) [51]	4.34	4.34
Body block losses (dB) [51]	10	10
Other losses (dB) [51]	10	10

Penetration loss(dB)	30.64	30.64
Slow fading margin (dB) [52]	8	8
Interference margin depend on the SINR [52]	0.5	1
16-QAM demodulation SINR (dB) [51]	-9	-9
Beam (500 users)(dB)	$-10\log_{10}(no\ of\ user)$	27

There are 500 user locations randomly selected in one base station, so receiver sensitivity is calculated as follows:

$$\text{Receiver sensitivity} = \text{thermal noise} + \text{Rx noise figure} + \text{demodulation threshold SINR} - 10\log_{10}(\text{no of user}) \qquad 3.18$$

Receiver sensitivity (RxS) = -154.93 + 7 -9-27 =-183.93

Path loss/link budget based on link budget parameters calculated as follows:

$$path\ loss = gNodeB\ Tx\ power - 10\ log_{10}(sub\ carrier\ quantity) + gNodeB\ antenna\ gain - gNodeB\ cable\ loss - body\ block\ loss - slow\ fading\ margin - foliage\ loss - rain\ margin - interference\ margin - atmospher\ loss - penetration\ loss - other\ losses + UT\ antenna\ gain - thermal\ noise\ figure - UT\ noise\ figure - 16 - QAM\ SINR\ (dB)$$

$$\text{for uplink Path loss(PL)} = 30 + 27 - 10 * \log_{10}(1584) - 2 - 10 - 8 - 10 - 4.34 - 3.45 - 0.5 - 30.64 + 21 + 154.93 - 7 + 9$$

=134.43dB

$$\text{for downlink Path loss(PL)} = 30 + 27 - 10 * \log_{10}(1584) - 2 - 10 - 8 - 10 - 4.34 - 3.45 - 10 - 30.64 + 21 + 154.93 - 7 + 9$$

=133.93dB

Therefore, the signal level at the receiver (link budget), dBm at each frequency in this thesis used the same parameters.

According to the calculation, the comparison between receiver signal level and receiver sensitivity is shown in the figure below. The receiver sensitivity is less than the receiver signal level, so it has passed for design.

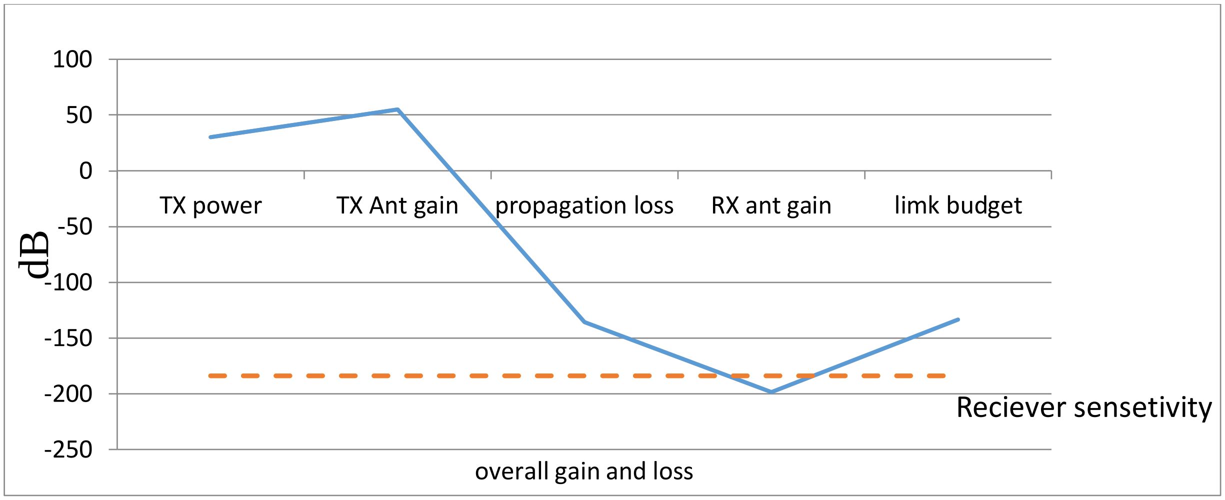

Figure 3.4: Comparison of receiver signal level or link budget vs receiver sensitivity

Figure 3.4 shows that the radio channel status is passed to design due to the signal level at the receiver (link budget) being greater than that of receiver sensitivity. Then the link budget is calculated and we have carrier frequency, so we calculate the cell radius (d) in meters by using the path loss formula. Propagation model path loss for dense urban scenarios 5GCM UMi-street canyon due to The NYUSIM simulator is used for all simulations in this study since it has been found to be more accurate than 3GPP, frequency in GHz and distance in meters.

Propagation model path loss for dense scenario 5GCM UMi-street canyon NLOS frequency in GHz and distance in meters.

$$PL = 22.4 + 35.3\log_{10}(d_{3D}) + 21.3\log_{10}(f_c) \qquad 3.19$$

$$distance(d3D) \quad = 10^{((link\ budget - 22.4 - 21.3\log_{10}(f_c))/35.3)}$$

Table 3.6: Distance (d3D) calculation results

Carrier frequency (GHz)	Downlink 5GCM UMi (d_{3D})(m)	Uplink 5GCM UMi (d_{3D}) (m)
73	108	112
28	193	200
4	625	646

$$d2D = \sqrt{((d3D)^2 - (hBs - hUT)^2)} \quad 4.19$$

Table 3.7: Distance (d2D) calculation results

Carrier frequency (GHz)	Downlink 5GCM UMi (d_{2D})(m)	Uplink 5GCM UMi (d_{2D}) (m)
73	107.67	111.68
28	192.8	199.82
4	624.56	645.57

After determine the cell size in x-y coordinate (d_{2D}), we can calculate the square area covered by one base station with good handover between the design gNodeB using below formula:

$$\text{coverage area} = 2.6 * d_{2D}^2 \quad 3.20$$

Table 3.8: Coverage area calculation result

Carrier frequency (GHz)	Coverage area(km^2) Downlink 5GCM UMi	Coverage area(km^2) of Uplink 5GCM UMi
73	0.03014135514	0.03242829824
28	0.09664678412	0.10381288424
Carrier frequency (GHz)	coverage area(km^2) Downlink 5GCM UMa	Coverage area(km^2) of Uplink 5GCM UMa
4	1.01419550336	1.08357762474010

Finally, determine the number of gNodeB based on link budget as follow as:

$$\text{5G gNodeB} = \left({}^{Total\ surface\ area\ of\ the\ cluster\ in\ Sq\ Km} / {}_{coverage\ Area\ of\ Single\ gNB} \right) \quad 3.21$$

Note I take Adama city in hectare 22165.86 when it changed to Sq. Km 221.66 km^2

Table 3.9: Number of gNodeB calculation result

Carrier frequency (GHz)	Downlink gNodeB	Uplink gNodeB
73	7354	6841
28	2295	2137
4	218	204

After calculating the number of gNodeB, they analysis performance of blockage sensitivity in mmwave cellular networks. The signal of mmwave is blocked by different materials, like concrete walls, which cause severe propagation loss. Therefore, microwave frequency bands have less sensitivity to blockage than mmwave frequency bands [53]. It causes NLOS/LOS blockage and a significant difference in path loss characterization [53]. These thesis indicate that mmwave is sensitive to blockage for three reasons. First, directionality is required; second, mmwave frequency does not diffract well in terrestrial environments; and third, high penetration loss while traveling through many common materials.

Considering cellular mobile networks in which base stations are placed according to a stochastic physical channel model with intensity on a Cartesian plan. We assume that the user starts from the origin and moves along the positive y-axis. Base stations, users, and the link between the users and base stations are three components of the system.

3.4.6.1 Base Stations

Assume that the set of base stations is denoted by Ψ where $b\ell$ represents the ℓ'Th base station and the polar coordinates of the base station in the x-y plane are denoted by (R_ℓ, φ_ℓ). Consequently, the base station sensitivity is given by λ, average size of the cell is given by $1/\lambda$.

3.4.6.2 Mobile Users

Starting at the origin, the user will travel along the positive y-axis starting from the origin at constant or variable speed. When using variable speed, the user's speed will fluctuate at random time intervals. Assume v_i and τ_i denote the user speed over the i'th interval and the duration of the i'th interval respectively. Assume that v_i is a speed range uniformly distributed $[a_i, b_i]$ and τ_i the parameters are exponentially distributed β_i. As it results, v_i and τ_i the probability density functions (pdfs) are:

$$f(v_i) = \frac{1}{(a_i + bi)}, \quad a_i < v_i < b_i, \qquad f(\tau_i) = \beta i e^{-\beta_i \tau_i}, \tau_i \geq 0 \qquad 3.22$$

The mean values of v_i and τ_i are given by,

$$\bar{\text{v}}\text{i} = \frac{1}{2}(a_i + b_i), \qquad \tau\bar{\text{i}} = \frac{1}{\beta_i} \qquad 3.23$$

Let the mean duration of the corresponding interval be inversely proportional to the absolute value of the difference between the user speed and the mean user speed over the interval.

$$\tau\bar{\text{i}} = \frac{\text{c}}{|v_i - \bar{\text{v}}\text{i}|} \qquad 3.24$$

Where c is the proportionality constant.

3.4.6.3 Link between the Base Stations and Users

Compute the SINR of uplink/downlink, it is being applied to directional beamforming, which is approximated by sector antenna pattern. From [34], the parameters of the sector antenna are given in the table 3.10, show that parameter of sector antenna which is main lobe directivity gain is donated by M , and back lobe directivity gain is denote by m directivity gain ,and θ the main lobe beam width. BS and U_T refer to base station and user terminal. The directivity gain between of the link between BS and U_T is donated by G_i and AoA and AoD of the link denote by ϕ_{UT} *and* $\phi\ t_{Bs}$. When angle of arrival and angle of departure is zero on other hands for interfering link uniformly distributed over the range$[0, 2\pi]$ the link is tagged to base station. $G_0 = M_B M_U$ The directivity gain of the tagged base station and for the interfering link i will be $G_i = a_k$ for $i > 0$ with probability pk, $k =$ 1,2,3,4, where a_k, p_k are defined in table 3.11 with $c_B = \frac{\theta_B}{2\pi}$ and $c_U = \frac{\theta_U}{2\pi}$.

Table 3.10: PDF of directivity gain G_i

k	1	2	3	4
a_k	$M_{Bs}M_{UT}$	$m_{Bs}M_{UT}$	$M_{Bs}m_{UT}$	$m_{Bs}m_{UT}$
p_k	$c_{Bs}c_{UT}$	$(1-c_{Bs})c_{UT}$	$c_{Bs}(1-c_{UT})$	$(1-c_{Bs})(1-c_{UT})$

Assume that the distance between Base station b_l and user when user starting from the origin is y-axis denote by $r_{l,y}$ and path loss exponent denote by $n_{l,y}$ and floating intercept of the path loss denoted $p_{l,y}$ of the corresponding link [54-56].

So $\alpha_{\ell,y}$ and $p_{\ell,y}$ floating intercept of the pathless depend on system carrier frequency of the system and has LOS/NLOS values. Signal of received power form BS [57, 58] is:

$$P_r = g_\ell P_T G_\ell p_{\ell,y} r_{\ell,y}^{-\alpha\ell,y} \qquad 3.25$$

σN^2 Constant additive noise power it dependent on user bandwidth of the system (B_W) and will be given.

$$\sigma N^2\,(dBm) = -174 + 10\log_{10} B_W + N_F \qquad 3.26$$

Where N_F is the noise figure in dB

$$\alpha_{k,y} = \begin{cases} 2 & if\ link\ r_{k,y}\ is\ LOS \\ 4 & if\ link\ r_{k,y}\ is\ NLOS \end{cases} \qquad 3.27$$

The probability mass function of (pmf) of random variable k then be determine .assume K denote the number of blockage over the link r_k, and Λ the blockage intensity. Blockage modeling as L length line segments, in [16], indicate that K has a stochastic distribution with mean$\gamma\tau_{(k,y)}$, where $\gamma = 2\Lambda/\pi[L]$.Thus LOS if the link does not have any obstruction otherwise it has NLOS. From the stochastic Poisson distribution. We determine the pmf of $a_{(k,y)}$ as follows:

$$prob(\alpha_k = 2) = (k = 0) = e^{-\gamma rk}$$

$$prob(\alpha_k = 4) = (k > 0) = 1 - e^{-\gamma rk} \qquad 3.28$$

The received information rate of the user is a variable since as the user travels along the y-axis its distances to the base stations change. T_{max} is threshold, $SINR_Y$ signal to interference plus noise ratio starting from y-axis.

$$C_y = B_W \ln(1 + \min(SINR_Y, T_{max})) \qquad 3.29$$

CHAPTER FOUR

4. SIMULATION RESULTS AND DISCUSSION

4.1 Simulation Parameters

The following is our simulation scenarios for outdoor-to-indoor mmwave propagation, which includes channel parameters and antenna specifications. For the UMi scenario, we simulated 28 GHz and 73 GHz frequencies with an 800 MHz bandwidth over 128 X 64 ULA antenna arrays MIMO channels. In addition, a 16 X 4 ULA antenna array is used to simulate 4 GHz with 200 MHz bandwidth for the UMa scenarios depending on the requirements of 3GPP 5G NR. All of the characteristics that affect mmwave propagation, including the large-scale parameters of Line-of-Sight (LOS), Non-Line-of-Sight (NLOS), analyzed the path loss, shadowing factor, and delay distribution depending on link budget parameters, as well as compared the penetration loss of buildings at different distances at 28 GHz.

Table 4.1: UMi and UMa scenarios, channel parameters and antenna features

Channel Parameters	Specification	
	UMi scenario	UMa scenario
Carrier frequency	28 GHz,73 GHz	4 GHz
bandwidth	800 MHz	200MHz
Height of BS	10m	25-30m
number of R_X	500	
Cell radius	112m,200, and 625 based on link budget calculation	
T_X power	30 dB	
T_X array type, Nt	ULA,128	ULA,16
R_X array type, Nr	ULA,64	ULA,4
T_X antenna spacing[59]	0.5λ	
R_X antenna spacing[59]	0.5λ	
modulation	OFDM	

Angle of Arrival and Departure [59]	7
Constant for ABG model(outdoor case)	Alpha α=3.4, Beta β=19.2 and Gamma γ=2.3 [9]
Constant for ABG model(indoor case)	Alpha α =4.17, Beta β=33 and Gamma γ=2.49 [9]

4.2 Simulation Results

The simulation uses three frequencies in the 5G system: 28 GHz and 73 GHz for the urban microcell (UMi) scenario with a radius of up to 112 and 200 meters respectively, and 4 GHz for the dense urban macrocell (UMa) environments with a cell size of up to 625 meters based on link budget calculation. Since path loss and shadowing are two of the most important variations in signal propagation that affect the received signal strength, the channel simulation results were used to get the values for these variations. Path loss and shadowing are caused by transmission distance and obstruction in the signal path in general. Thus, analyze these differences for LOS and NLOS scenarios under directional and omnidirectional path loss. Directional and omnidirectional conditions power delay profiles (PDP) for each considered frequency are compared to NLOS scenarios. Also, penetration loss is simulated as follows:

4.2.1 Performance Analysis of Penetration Loss

The penetration loss properties of the materials used in the building have a big impact on wireless coverage. As a result, the penetration loss properties of different building materials that are currently available. Penetration loss properties at very high frequencies, with a focus on the 5G cellular network. Based on the type of material, the penetration loss of building materials varies greatly. Penetration loss has been shown to rise with frequency in most cases. Any materials estimated penetration loss was found to be consistent with their calculated penetration loss. In buildings, penetration loss is expected to improve SINR, leading to an improvement in the data rate of users. It is very important to estimate how many improvements in data rate may take place. Therefore, MATLAB based simulation analysis has been performed to simulate the data rate experience of the user. The analysis considered 5G systems, and so, the range of frequency bands up to 100 GHz.

In simulation, three different distances between the user and the base station were used. In figures 4.1, 4.2, and 4.3, they show the simulation results for distances of 60, 80, and 100 meters, respectively. In all of the results, the approach clearly increases the data rate. When we use high BPL, the data rate is high at low frequency and when the distance between the user and the base station is small. But at high frequency and when the distance between the base station and the user increases, it is equal to the low and high BPL data rate. The data rate varies widely, but with an irregular frequency, as seen in figure 4.1-4.3. However, at high frequencies or above 60 GHz, both low BPL and high BPL performance gradually decline.

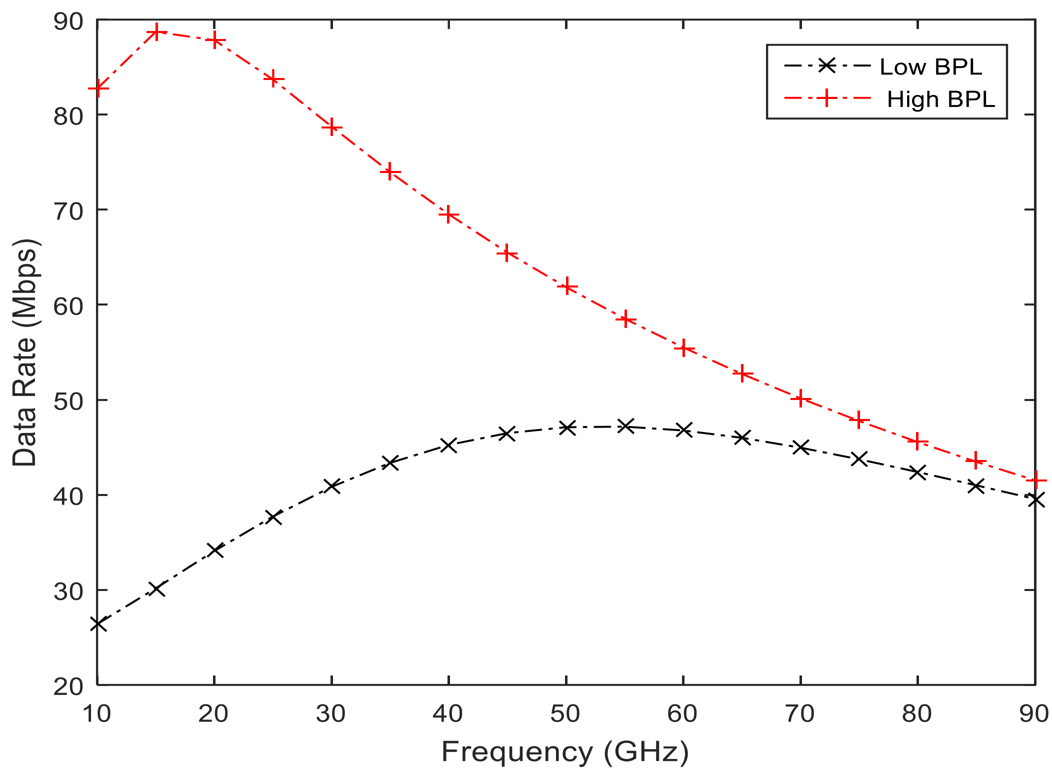

Figure 4.1: Data Rate (Mbps) vs. Frequency (GHz) user 60 m away from base station

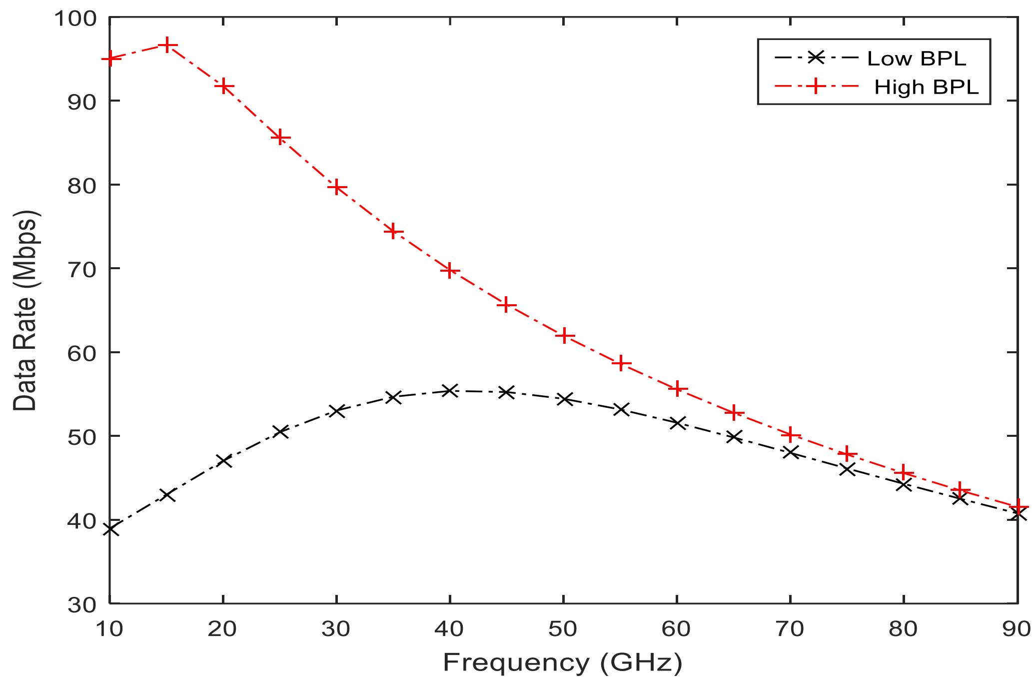

Figure 4.2: Data Rate (Mbps) vs. Frequency (GHz) user 90 m away from base station

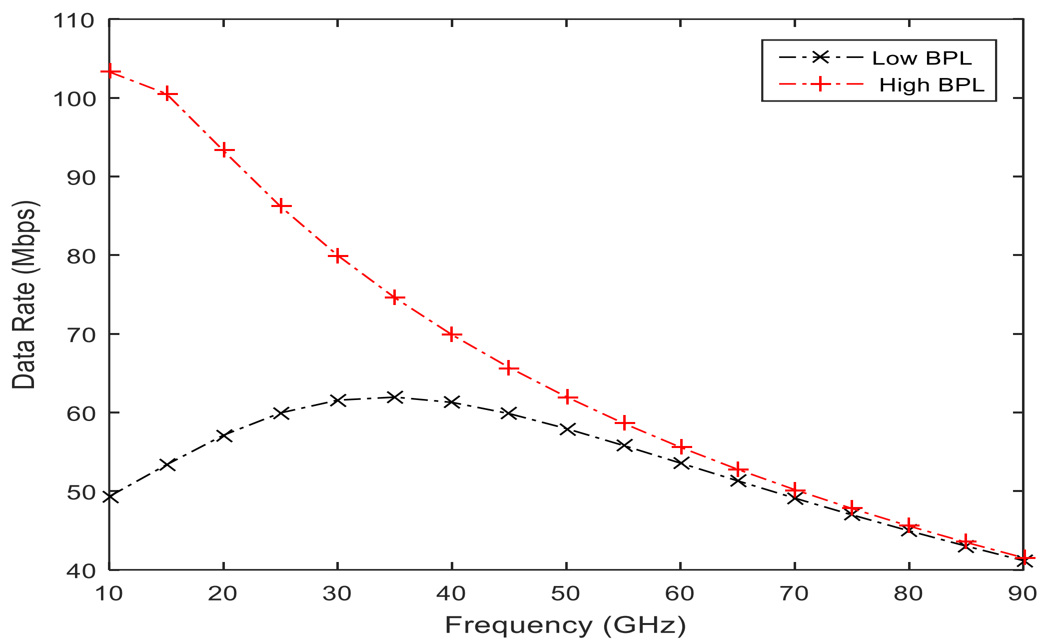

Figure 4.3: Data Rate (Mbps) vs. Frequency (GHz) user 100 m away from base station

Figure 4.4 shows average information rates (Gbps) as a function of user distance from the origin with blockage intensity of an average cell size (radius) of 200 m. The information rate fluctuates as the user travels from one base station to another, as shown in the figure. The user has more handover from neighboring cells and data rate when the cell radius of the cell is small and the blockage intensity is strong. The identified base station changes when traveling small distances (segments), as it analysis which BS is LOS at each location and tries to connect the BS. If all BS are located in non-line of sight, they connect to the BS at the shortest distance.

At a distance of around or approximately 740-790m, there is a significant increase in the rate of information, as seen in figure 4.4. When all of the BS that interferes becomes NLOS, only the identified or labeled BS remains LOS, this type of spike appears. In this situation, the interference is quite low, leading to a very high flow of information or data rate.

Figure 4.5 indicates that identified or labeled BSs NLOS/LOS state. LOS is represented by '1', and NLOS is represented by '2'. It can be analyzed. The identified user is located at an average LOS and NLOS.

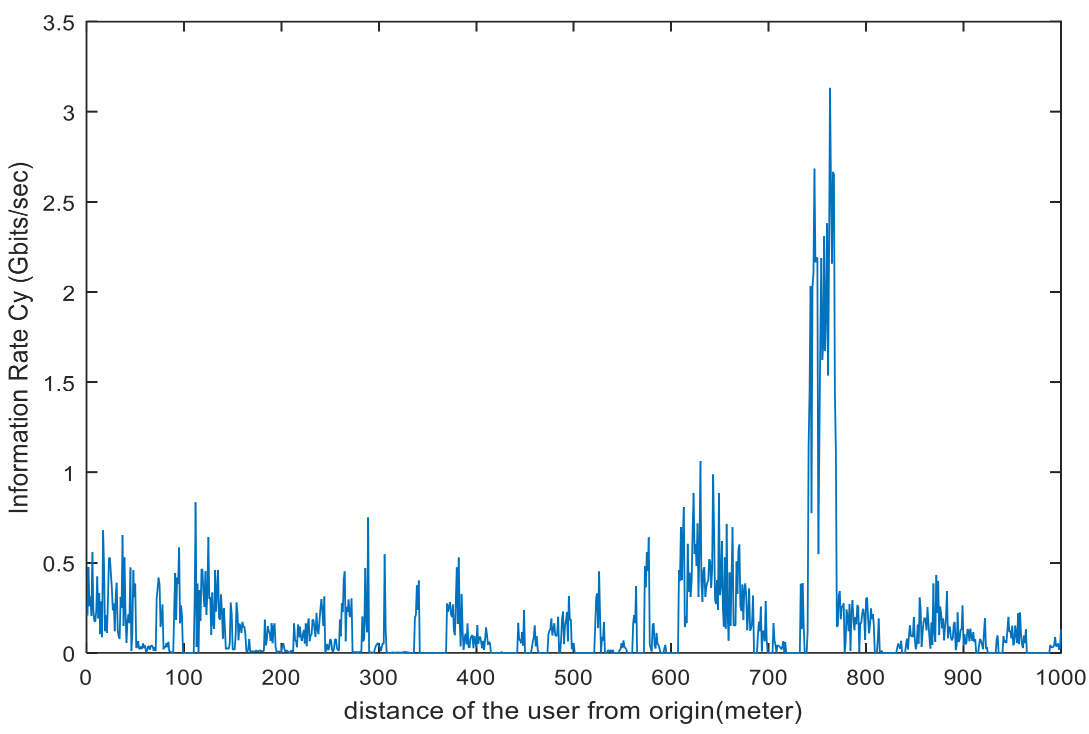

Figure 4.4: Average information rate (Gbps) vs user distance to origin for 200 m cell radius with 1 m/s user speed

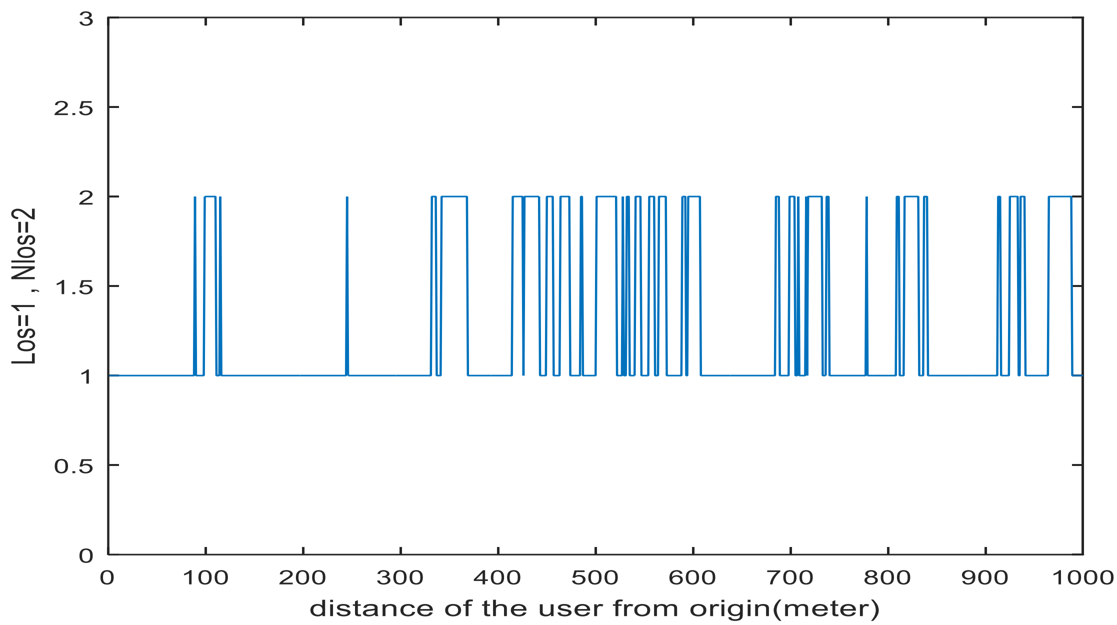

Figure 4.5: The tagged base station is LOS or NLOS vs user distance from the organ with cell radius of 200m user speed 1m/s

4.3 Dense Urban Microcell (UMi) Scenario

The two main characteristics of dense urban areas are high traffic loads, and outdoor and outdoor-to-indoor coverage. Consideration of the high penetration loss at mmWave Examine the efficiency of the 4, 28, and 73 GHz bands with T_X-R_X distances of 625,200 and 112 meters based on link budget calculation using the same parameters, respectively, for both LOS and NLOS cases in this section, based on link budget calculation. The performance will be evaluated in both directional and omnidirectional scenarios. The PDP of NLOS scenarios are also discussed under directional and omnidirectional scenarios for each use frequency at a randomly chosen T_X-R_X distance.

4.3.1 Performance Analysis at 28 GHz

The carrier frequency in this simulation is the frequency band of 28 GHz, which has a lot of interest and popularity for future mmwave communication [22]. For LOS and NLOS scenarios, figure 4.6 shows the simulation results for directional and omnidirectional path loss, aggregated path loss exponents (PLE), and directional best. As the lower and upper bound of the T_X, the figure shows the efficiency of 5GCM at 500 users randomly selected R_X ranging from 10m to 200m of cell radius.

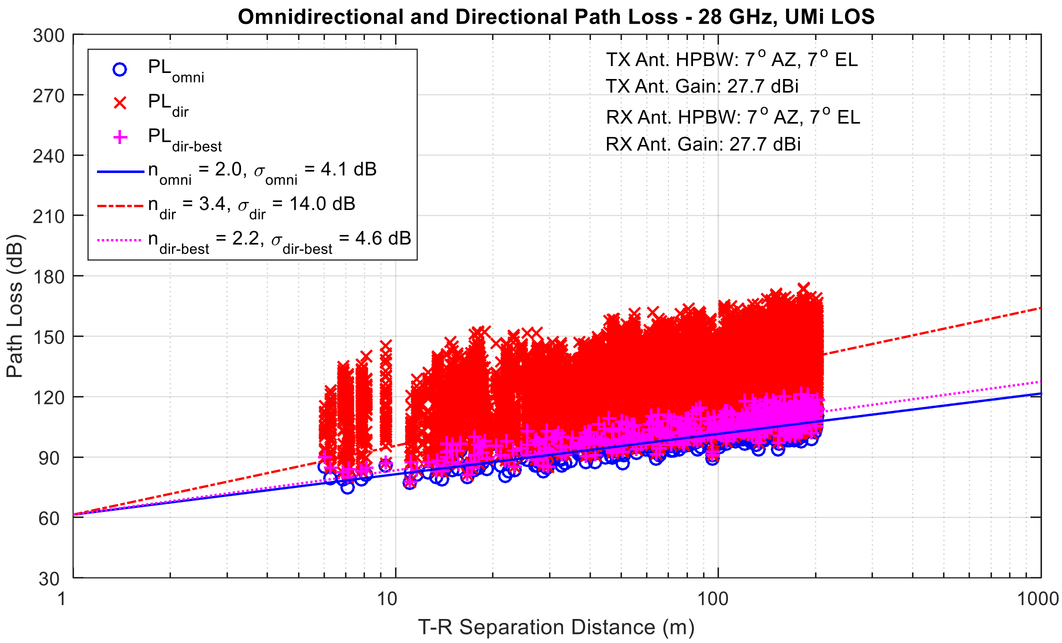

(a)

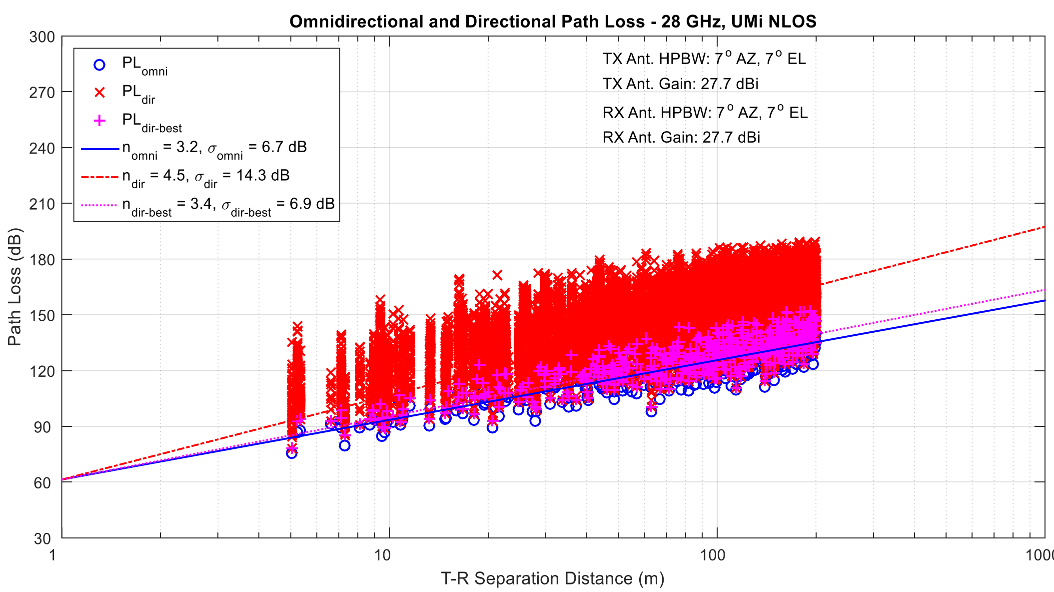

(b)

Figure 4.6: Omnidirectional and directional path loss simulation results for 28 GHz UMi, (a) LOS (b) NLOS scenarios

The path loss increases linearly with distance in figure 4.6, and it is higher for directional propagation in both scenarios, and it is significantly higher under NLOS scenarios. The directional PLE of 3.4 with a shadowing factor (SF) of dir=14.0 dB is higher than the omnidirectional PLE of 2.0 with a shadowing factor of omni=4.1dB for LOS, as shown in figure 4.6 (a). The directional best PLE, or the strongest feasible link generated on a directed path, is, on the other hand, quite near to the omnidirectional PLE. Furthermore, as shown in Figure 4.6 (b), path loss increases in the NLOS scenarios than in the LOS scenarios when the signal path is obstructed. The directional path PLE increases to 4.5 in the NLOS case, with a shadowing factor of 14.3 dB, although the directional best value is 0.2 dB, both PLE and SF are greater than in omnidirectional propagation. Higher directional PLE for both NLOS and LOS situations at 28 GHz is likely due to antenna arrays not being optically aligned on boresight, according to the results. On the other hand, the directional best PLE, or the strongest possible link generated on the directed path, is very close to the omnidirectional PLE. The path loss occurs higher in the NLOS conditions than in the LOS conditions when the signal path is obstructed, as shown in figure 4.6 (b). Although the directional best value is 0.2 dB, the directional path loss increases to 4.5 in the NLOS conditions with shadowing factors of 14.3 dB. Both PLE and SF are higher than in omnidirectional propagation. As per the results, higher directional PLE for both NLOS and LOS scenarios at 28 GHz is likely due to the antenna array not being optimally aligned on boresight. Steerable beam antennas can be used to solve this problem [60].

The results also suggest that under the UMi scenarios, omnidirectional propagation path loss at 28 GHz is not significantly higher than in the current microwave system. Furthermore, the angle of arrival and departure is inversely proportional to T_X and R_X antenna gain. Which means when the angle of arrival and departure is small, the T_X and R_X antenna gain increase and when the angle of arrival and departure increases, the T_X and R_X antenna gain increase due to narrow beamforming.

The Directional Power delay profile (PDP) with the strongest power and omnidirectional PDP for the 28 GHz in the UMi NLOS scenario at a randomly chosen R_X location of 201.2m is shown in figure 4.7. The path loss and PLE for both directional and omnidirectional situations indicate only a minor difference. As can be indicated for the RMS delay spread (σ_τ) with a time difference for directional PDF with strongest power 0.4ns and for omnidirectional 10.2ns, The received signal power for omnidirectional, on the other hand, is more than twice as low as for directional.

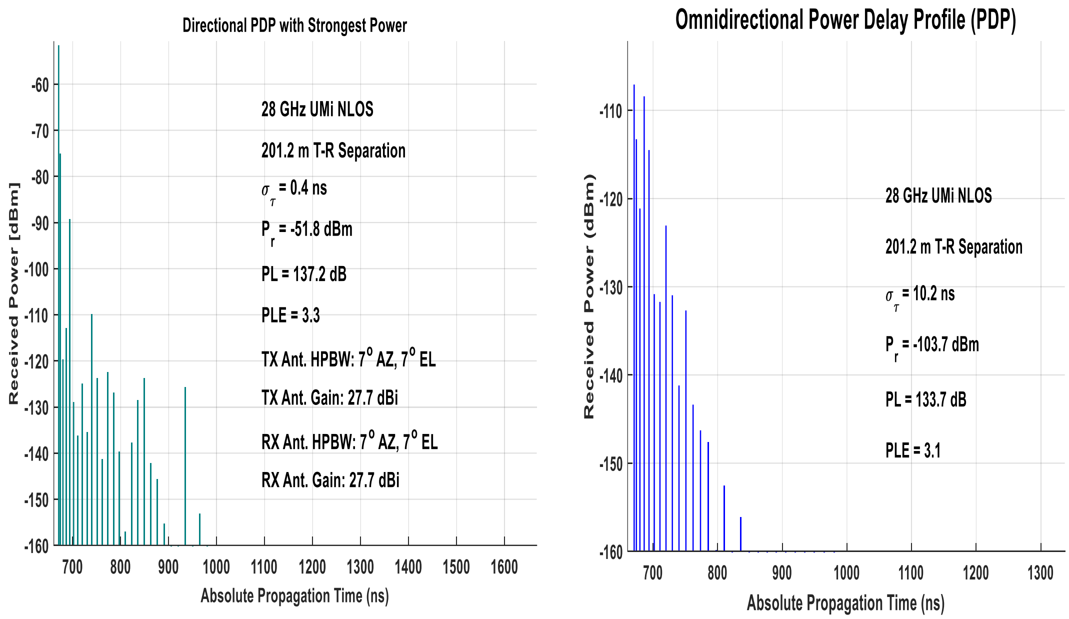

Figure 4.7: UMi NLOS omnidirectional PDP and directional PDP, with strongest power at 28 GHz and T_X and R_X ranging to 201.2m

4.3.2 Performance Analysis at 73 GHz

The 73 GHz band is another common frequency which has attracted the interest of academia for industry and research applications. At 73 GHz, researchers were able to achieve a multi-Gigabit per second wireless network at 73 GHz, which has also been used in 5G trials by several companies. In urban areas, it is still a popular frequency band for 5G testing or deployment in urban areas. Figure 4.8 shows the omnidirectional, directional path loss, and directional best PLE for the simulation results for the LOS and NLOS scenarios in the 73 GHz band.

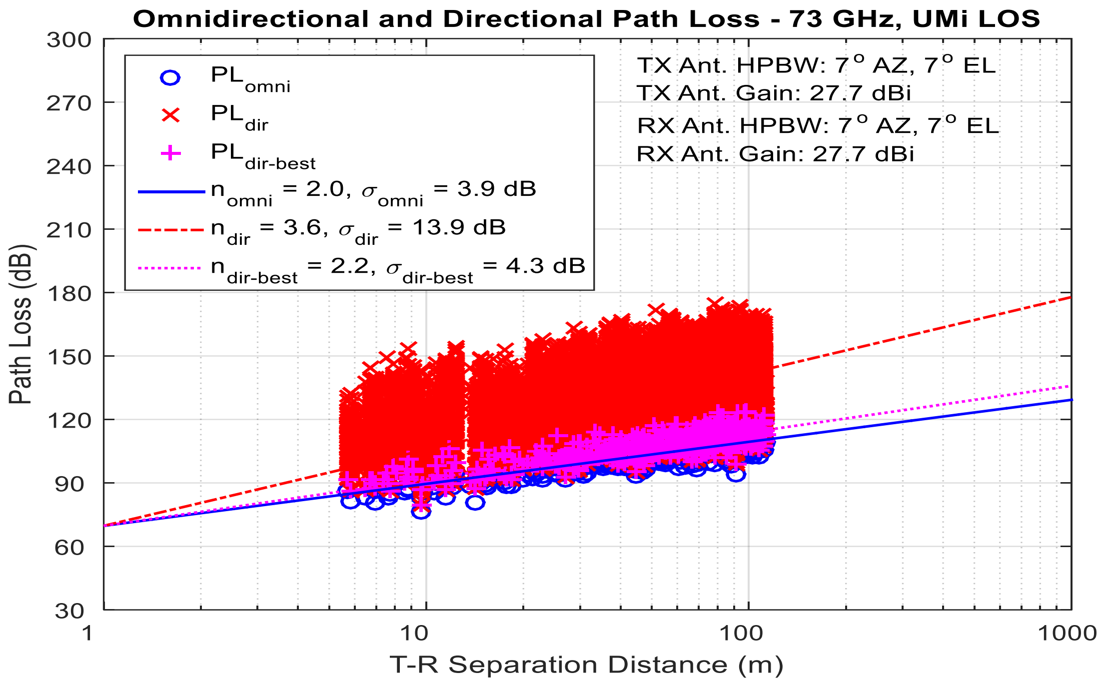

(a)

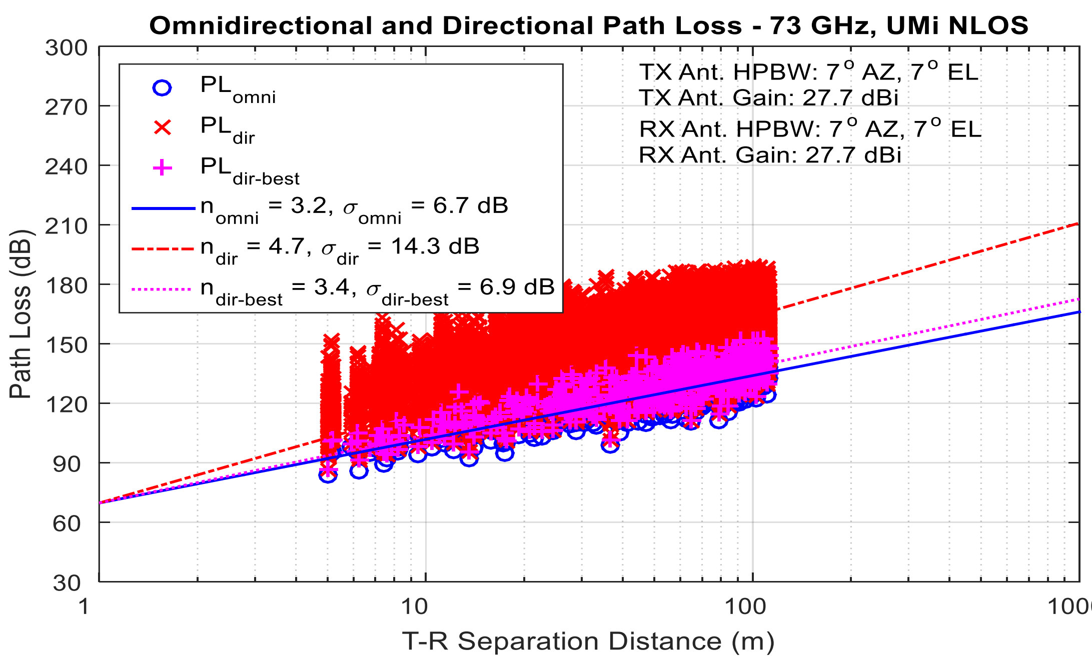

(b)

Figure 4.8: 73 GHz UMi, (a) LOS and (b) NLOS scenarios, to perform omnidirectional and directional path loss values

In both cases, path loss increases linearly with distance and is higher for direction propagation, as shown in figure 4.8.The SF and PLE at 73 GHz are smaller than at 28 GHz under identical channel parameters, as shown in figure 4.8 (a). According to the simulation results, cellular networks in dense urban environments can use 73 GHz, which is suitable for both LOS and NLOS in ISDs less than 112 m.

Figure 4.9 shows the PDP for omnidirectional and directional propagation at 73 GHz at 112 m. A minor difference exists between PLE and PL similar to 28 GHz. However, in this UMi NLOS condition, the ratio of omnidirectional to directional delays spreads in the order of 55 times, implying that omnidirectional has long time delays than directional, which is larger than measurement data [61]. As per the finding, the omnidirectional delay spread for NLOS at 73 GHz is larger, and it receives a much larger number of multipath components than directional propagation.

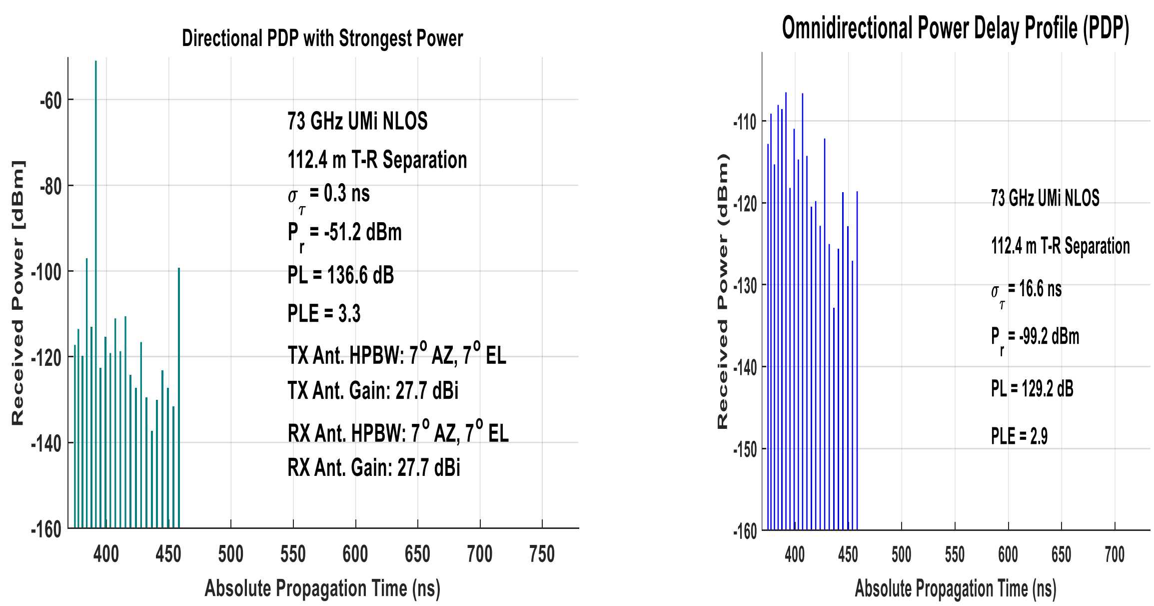

Figure 4.9: Omnidirectional and directional propagation PDF at 73 GHz with a T_X-R_X separation at 112.4 m

4.3.3 Performance Analysis at 4 GHz

The ISD of this scenario is up to 200m, but since 4 GHz used 625m based on cell radius calculation using the ABG path loss model that is used for urban macrocells (UMa). Recently, the 4 GHz band has received much interest as one of the bands that will be assigned for 5G in WRC-19. Field measurements and tests on this frequency have already begun in some countries, such as Japan [19].

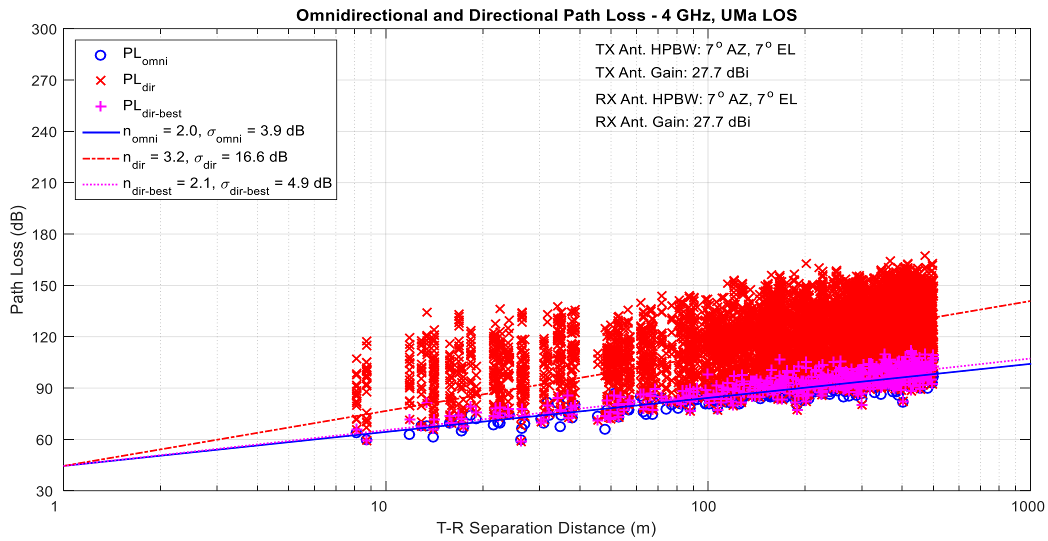

(a)

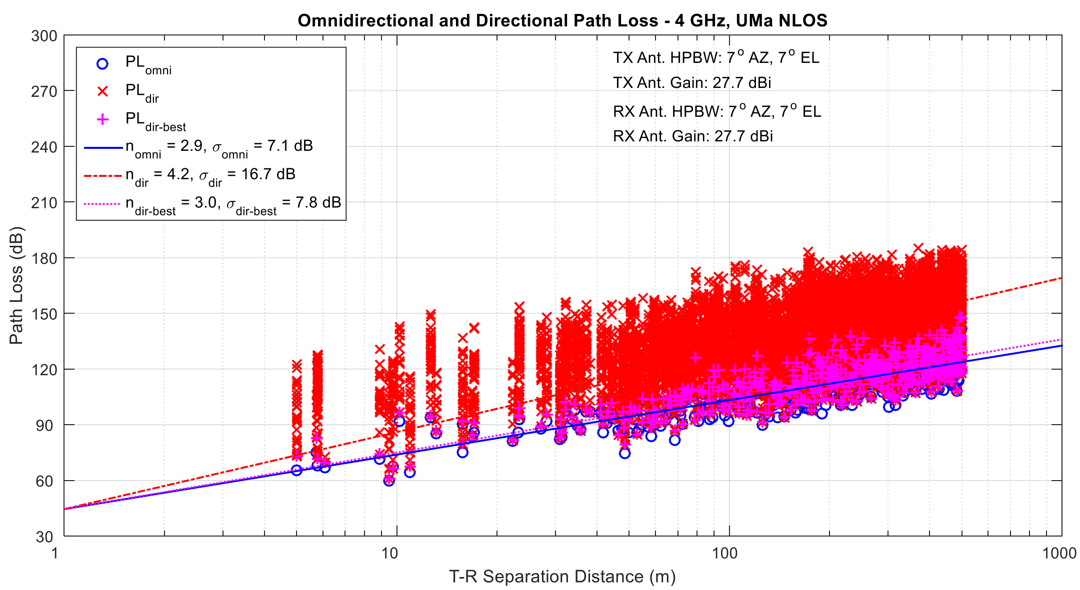

(b)

Figure 4.10: Directional and omnidirectional path loss values for the 4 GHz UMa, (a) LOS and (b) NLOS scenarios

Since 4 GHz is a sub-6 GHz band, a wide bandwidth of up to 200 MHz can be used in this band for 5G applications, according to the 3GPP [40] recommendation. The PLE of both LOS and NLOS at 4 GHz is similar or approximately to 28 GHz and 73 GHz, as shown in Figure 4.10 (b). The SF at dir=16.7 dB, however, is greater than both previous frequencies, as shown in Figure 4.10 (a). Similarly, the shadow factor for NLOS is higher than for other frequencies studied. Figure 4.11 shows the directional and omnidirectional power delay profiles for the 626.9 m UMa NLOS scenario with the strongest power at 4 GHz.

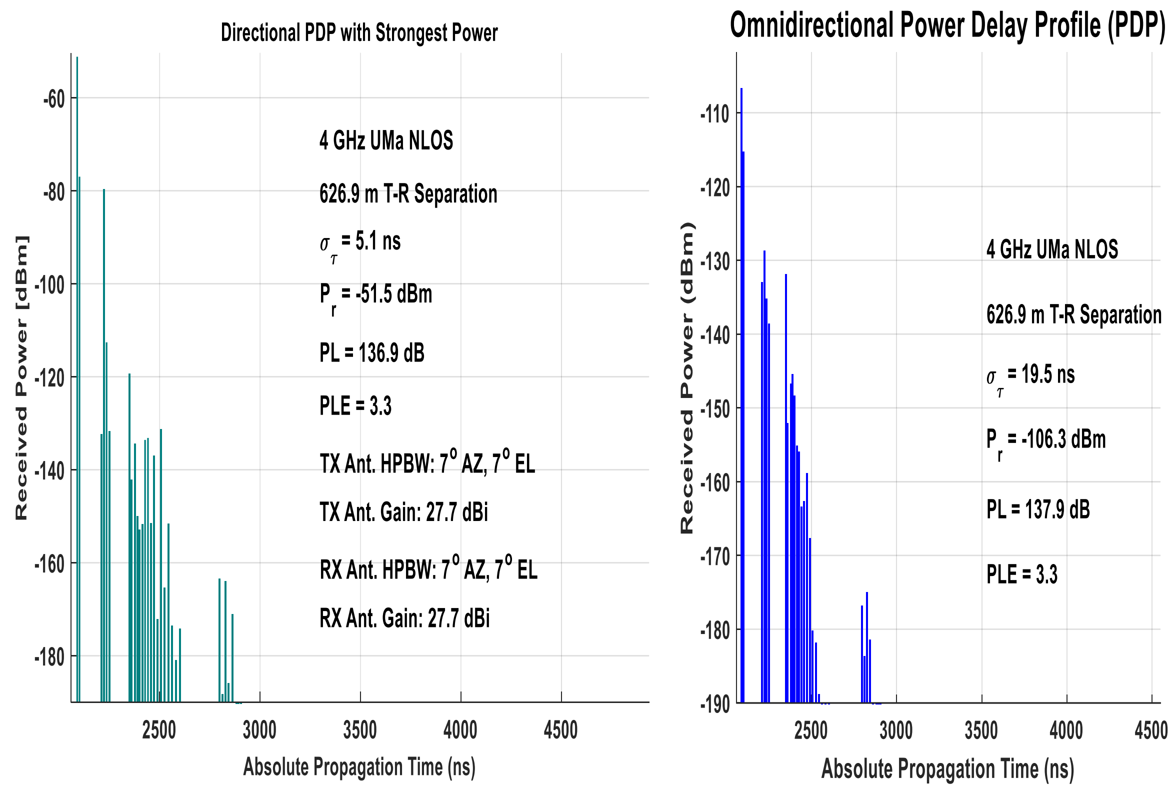

(a) (b)

Figure 4.11: The omnidirectional and directional propagation PDF at 4 GHz with a T_X-R_X separation at 626.9 m

Figure 4.11 shows the PDP for directional and omnidirectional propagation at 4 GHz with a T_X-R_X separation of 626.9 m. The PLE and PL have the same value in each case, similar to 28 GHz and 73 GHz. The ratio of omnidirectional to directional delay spread in these UMa NLOS conditions, on the other hand, is in the order of 150 times. The results show that in the NLOS scenarios at 4 GHz around 625m, the number of multipath components can be recognized with path loss comparable to other mmwave frequencies. In table 4.3, the path loss calculated based on link budget parameters is less than simulation results at each frequency band except for the 73 GHz omnidirectional power delay profile, and there is a small change in distance between the simulation and calculation results.

Table 4.2: Simulation result Comparison of omnidirectional, directional best and directional path loss at 73 GHz, 28 GHz, and 4 GHz

Parameters comparison	73 GHz		28 GHz		4 GHz	
	LOS	NLOS	LOS	NLOS	LOS	NLOS
PLE(omnidirectional)	2	3.2	2	3.1	2	2.9
PLE(directional best)	2.2	3.4	2.2	3.4	2.1	3
PLE(directional)	3.6	4.7	3.4	4.5	3.2	4.2
shadow fading(omnidirectional)	3.9	6.7	4.1	6.7	3.9	7.1
shadow fading(directional best)	4.3	6.9	3.6	6.9	4.9	7.8
shadow fading(directional)	13.9	14.3	14	14.3	16.6	16.7

Table 4.3: Simulation result PDP for directional and omnidirectional propagation at 73 GHz, 28 GHz, and 4 GHz

Power delay profile parameters	73 GHz		28 GHz		4 GHz	
	Omnidirectional	directional with strongest power	Omnidirectional	directional with strongest power	omnidirectional	directional with strongest power
time delay(ns)	16.6	0.3	10.2	0.4	19.5	5.1
Path loss(dB)	129.2	136.6	133.7	137.2	137.9	136.9
power received(dBm)	-99.2	-51.2	-103.7	-51.8	-106.3	-51.5

The finding of this thesis analysis mmwave frequency bands can be utilized in the 5G mobile network by solving certain propagation problems in all circumstances. According to simulation results, microcell propagation in both LOS and NLOS. In all cases, the considered mmWave frequency bands are compensable for being used in a 5G mobile network by solving certain propagation problems. The results also show that for 5G access transmission, microcells based cell radius, close to 112, 200, and 625 m, for 73, 28, and 4 GHz respectively, would be enough for 5G access transmission. According to the simulation results, the PL and SF decrease from high frequency to low frequency and time delay increase as the distance increase or frequency decrease, as well as the path loss of directional path loss is higher than that of omnidirectional.

CONCLUSIONS

In 5G and beyond networks, millimeter wave communication is vital for the internet of things in 5G and beyond networks. The propagation analysis of mmWaves in dense urban areas for 5G cellular networks was discussed in this thesis. The results of this thesis show that mmwave could be used in 5G cellular outdoor-to-indoor networks to overcome some propagation problems and provide massive connectivity in densely populated areas.

Millimeter waves have high propagation loss and are more sensitive to blockage than standard wireless communications, according to the propagation properties of millimeter waves. At a high frequency. The coverage or cell size is reduced. Both low BPL and high BPL performance gradually decline as the distance between the base stations and user's increases. The efforts to model mmWave channels were discussed, and various channel models that had been developed are included. Additionally, they looked over the specifics of the channel model considering densely populated urban areas.

Finally, we analyzed the performance of the 4 GHz, 28 GHz and 73 GHz mmwave bands performed in dense UMi and UMa areas. The simulation results show that the path loss in this environment is within the compensable range for propagation in both LOS and NLOS instances. However, in the LOS and NLOS scenarios for directional propagation, the path loss is larger than in the omnidirectional case, and it increases rapidly as the distance increases. The directional has fewer time delays and higher receiving power than the omnidirectional. Furthermore, analyzing mmwave frequency bands' large–scale characteristics has shown a significant capability for use in dense urban areas. To solve severe path loss problems, in some cases, massive MIMO with high gain directional antenna arrays is required.

FUTURE WORKS

- Analysis of the absorption effect, ceiling reflection, and ground human body in various indoor scenarios for example ceramic flooring, marble, wood, and carpeted.
- Analysis of known building materials characteristics at different mmwave frequency bands propagation, which means the value of extracted parameters is mainly dependent on environmental conditions.
- Analysis measurement of conducting channel parameters in mostly outdoor and indoor environments, for example, industrial zones, airports and train stations.

REFERENCE

[1] I. A. Hemadeh, K. Satyanarayana, M. El-Hajjar, and L. Hanzo, (2017)."Millimeter-wave communications: Physical channel models, design considerations, antenna constructions, and link-budget," *IEEE Communications Surveys & Tutorials,* vol. 20, no. 2, pp. 870-913.

[2] A. Gupta and R. K. Jha, (2015)."A survey of 5G network: Architecture and emerging technologies," *IEEE access,* vol. 3, pp. 1206-1232.

[3] T. S. Rappaport *et al.,* (2013). "Millimeter wave mobile communications for 5G cellular: It will work!," *IEEE access,* vol. 1, pp. 335-349.

[4] J. Zhang, X. Ge, Q. Li, M. Guizani, and Y. Zhang, (2016)."5G millimeter-wave antenna array: Design and challenges," *IEEE Wireless communications,* vol. 24, no. 2, pp. 106-112.

[5] P. K. Agyapong, M. Iwamura, D. Staehle, W. Kiess, and A. Benjebbour, (2014)."Design considerations for a 5G network architecture," *IEEE Communications Magazine,* vol. 52, no. 11, pp. 65-75.

[6] H. Zhao *et al.,* (2013)."28 GHz millimeter wave cellular communication measurements for reflection and penetration loss in and around buildings in New York city," in *2013 IEEE international conference on communications (ICC),* IEEE, pp. 5163-5167.

[7] R. El Hattachi and J. Erfanian, (2015)."NGMN 5G white paper," *NGMN Alliance, February*.

[8] S. Sun, G. R. MacCartney, and T. S. Rappaport, (2016)."Millimeter-wave distance-dependent large-scale propagation measurements and path loss models for outdoor and indoor 5G systems," in *2016 10th European Conference on Antennas and Propagation (EuCAP),* IEEE, pp. 1-5.

[9] N. Docomo, (Oct,,2016)."5G Channel Model for bands up to100 GHz," Tech. Report.

[10] I. M. Rafiqul, M. L. Altajjar, M. S. Habib, K. Abdullah, M. M. Rashid, and K. L. Bashar, (2015). "Frequency diversity improvement factor for rain fade mitigation in Malaysia," in *2015 IEEE International WIE Conference on Electrical and Computer Engineering (WIECON-ECE),* IEEE, pp. 159-163.

[11] T. S. Rappaport, F. Gutierrez, E. Ben-Dor, J. N. Murdock, Y. Qiao, and J. I. Tamir, (2012)."Broadband millimeter-wave propagation measurements and models using

adaptive-beam antennas for outdoor urban cellular communications," *IEEE transactions on antennas and propagation,* vol. 61, no. 4, pp. 1850-1859.

[12] T. S. Rappaport, G. R. MacCartney, M. K. Samimi, and S. Sun, (2015)."Wideband millimeter-wave propagation measurements and channel models for future wireless communication system design," *IEEE transactions on Communications,* vol. 63, no. 9, pp. 3029-3056.

[13] F. Marzouk, J. P. Barraca, and A. Radwan, (2020)."On Energy Efficient Resource Allocation in Shared RANs: Survey and Qualitative Analysis," *IEEE Communications Surveys & Tutorials,* vol. 22, no. 3, pp. 1515-1538.

[14] T. Wu, T. S. Rappaport, and C. M. Collins, (2015)."The human body and millimeter-wave wireless communication systems: Interactions and implications," in *2015 IEEE International Conference on Communications (ICC)*, IEEE, pp. 2423-2429.

[15] A. Goldsmith, *Wireless communications*. Cambridge university press, 2005.

[16] P. Pirinen, (2014: IEEE)."A brief overview of 5G research activities," in *1st International Conference on 5G for Ubiquitous Connectivity*, pp. 17-22.

[17] P. Goyal and A. K. Sahoo, (2019) "A roadmap towards connected living: 5G mobile technology," *Int. J. Innov. Technol. Explor. Eng,* vol. 9, no. 1, pp. 1670-1685, 2019.

[18] C. Antón-Hero and X. Mestre, (2020: IEEE)"Advanced Learning Architectures and Spatial Statistics for Beam Selection with Multi-Path," in *GLOBECOM 2020-2020 IEEE Global Communications Conference*, pp. 1-6.

[19] A. S. Seraj, (2019)."Study on Propagation Characteristics of 5G Millimeter-Wave Wireless Communication Systems for Dense Urban Environments," Waseda University.

[20] K. Smith, (2020: IEEE)"Implementing RINA in 5G networks," in *2020 23rd Conference on Innovation in Clouds, Internet and Networks and Workshops (ICIN)*, pp. 46-50.

[21] Y. Niu, Y. Li, D. Jin, L. Su, and A. V. Vasilakos, (2015). "A survey of millimeter wave communications (mmWave) for 5G: opportunities and challenges," *Wireless networks,* vol. 21, no. 8, pp. 2657-2676.

[22] W. Xiang, K. Zheng, and X. S. Shen, (2016).*5G mobile communications*. Springer.

[23] I. Afolabi, A. Ksentini, M. Bagaa, T. Taleb, M. Corici, and A. Nakao, (2017). "Towards 5G network slicing over multiple-domains," *IEICE Transactions on Communications,* vol. 100, no. 11, pp. 1992-2006.

[24] M. Marcus and B. Pattan, (2005)."Millimeter wave propagation: spectrum management implications," *IEEE Microwave Magazine,* vol. 6, no. 2, pp. 54-62.

[25] V. Kristem *et al.*, (2017)."3D MIMO outdoor-to-indoor propagation channel measurement," *IEEE Transactions on Wireless Communications,* vol. 16, no. 7, pp. 4600-4613.

[26] X. Ge, L. Pan, S. Tu, H.-H. Chen, and C.-X. Wang, (2016: IEEE). "Wireless backhaul capacity of 5G ultra-dense cellular networks," in *2016 IEEE 84th Vehicular Technology Conference (VTC-Fall)*, pp. 1-6.

[27] A. Aijaz, (2020)."Private 5G: The future of industrial wireless," *IEEE Industrial Electronics Magazine,* vol. 14, no. 4, pp. 136-145.

[28] K. Sakaguchi *et al.*, (2017)."Where, when, and how mmWave is used in 5G and beyond," *IEICE Transactions on Electronics,* vol. 100, no. 10, pp. 790-808.

[29] M. K. Samimi, G. R. MacCartney, S. Sun, and T. S. Rappaport, (2017: IEEE)"28 GHz millimeter-wave ultrawideband small-scale fading models in wireless channels," in *2016 IEEE 83rd Vehicular Technology Conference (VTC Spring)*, pp. 1-6.

[30] Z. Pi and F. Khan, (2011). "An introduction to millimeter-wave mobile broadband systems," *IEEE communications magazine*, vol. 49, no. 6, pp. 101-107.

[31] R. C. Daniels, J. N. Murdock, T. S. Rappaport, and R. W. Heath, (2010). "60 GHz wireless: Up close and personal," *IEEE Microwave magazine,* vol. 11, no. 7, pp. 44-50.

[32] M. Benisha, R. T. Prabu, and V. T. Bai, (2016: IEEE)"Requirements and challenges of 5G cellular systems," in *2016 2nd International Conference on Advances in Electrical, Electronics, Information, Communication and Bio-Informatics (AEEICB)*, pp. 251-254.

[33] P. Adhikari, (2008). "Understanding millimeter wave wireless communication," *Loea Corporation*, pp. 1-6.

[34] T. Bai and R. W. Heath, (2014)."Coverage and rate analysis for millimeter-wave cellular networks," *IEEE Transactions on Wireless Communications,* vol. 14, no. 2, pp. 1100-1114.

[35] S. Salous, (2013), *Radio propagation measurement and channel modelling*. John Wiley & Sons.

[36] G. R. Maccartney, T. S. Rappaport, S. Sun, and S. Deng, (2015)."Indoor office wideband millimeter-wave propagation measurements and channel models at 28 and 73 GHz for ultra-dense 5G wireless networks," *IEEE access,* vol. 3, pp. 2388-2424.

[37] G. R. MacCartney, J. Zhang, S. Nie, and T. S. Rappaport, (2013: IEEE)."Path loss models for 5G millimeter wave propagation channels in urban microcells," in *2013 IEEE global communications conference (GLOBECOM)*, pp. 3948-3953.

[38] M. Samimi *et al.*, (2014: IEEE)."28 GHz angle of arrival and angle of departure analysis for outdoor cellular communications using steerable beam antennas in New York City," in *2013 IEEE 77th Vehicular Technology Conference (VTC Spring)*, pp. 1-6.

[39] A. Ghosh, (2015). "5G channel model for bands up to 100 GHz," *5GCM white paper*.

[40] V. V. Díaz and D. M. Aviles, (2018: IEEE). "A path loss simulator for the 3GPP 5G channel models," in *2018 IEEE XXV International Conference on Electronics, Electrical Engineering and Computing (INTERCON)*, pp. 1-4.

[41] I. Rodriguez, O. Koymen, A. Partyka, and J. Järveläinen, "Propagation Path Loss Models for 5G Urban Micro-and Macro-Cellular Scenarios."

[42] M. Tanvir Kawser, (2018)."Determination of penetration losses of various building materials to help design a building with better wireless services," 2018.

[43] M. S. Ahmad, N. A. Kabir, S. Nursakinah, A. A. Oglat, H. Thabit, and S. L. Zeyadeh(2018)., "Radioluminescence and scintillation properties of zinc doped with aluminum," *Int J Chem Pharm Technol,* vol. 3, pp. 44-9.

[44] R. M. Buchter, (2018). "2020: faster than real-time tactical intelligence, surveillance, and reconnaissance (ISR) from the dismount, and faster than real-time strategic ISR to the dismount," in *Ground/Air Multisensor Interoperability, Integration, and Networking for Persistent ISR IX*, vol. 10635: International Society for Optics and Photonics, p. 106350I.

[45] T. Lee, J. Yoon, S. Lee, and J. Shin, (2010: IEEE)."Resource allocation analysis in OFDMA femtocells using fractional frequency reuse," in *21st annual IEEE*

international symposium on personal, indoor and mobile radio communications, pp. 1224-1229.

[46] K. Haneda *et al.* (2016: IEEE). "5G 3GPP-like channel models for outdoor urban microcellular and macrocellular environments," in *2016 IEEE 83rd vehicular technology conference (VTC spring)*, pp. 1-7.

[47] T. S. Rappaport, S. Sun, and M. Shafi, (2017: IEEE). Investigation and comparison of 3GPP and NYUSIM channel models for 5G wireless communications," in *2017 IEEE 86th vehicular technology conference (VTC-Fall)*, pp. 1-5.

[48] T. S. Rappaport, (2018). "5G Millimeter Wave Wireless: Trials, Testimonies, and Target Rollouts," in *IEEE Infocom*.

[49] T. S. Rappaport, Y. Xing, G. R. MacCartney, A. F. Molisch, E. Mellios, and J. Zhang, (2017)."Overview of millimeter wave communications for fifth-generation (5G) wireless networks—With a focus on propagation models," *IEEE Transactions on antennas and propagation*, vol. 65, no. 12, pp. 6213-6230.

[50] S. Sun *et al.*, (2016: IEEE). "Propagation path loss models for 5G urban micro-and macro-cellular scenarios," in *2016 IEEE 83rd Vehicular Technology Conference (VTC Spring)*, pp. 1-6.

[51] H. Ganame, L. Yingzhuang, H. Ghazzai, and D. Kamissoko, (2019). "5G base station deployment perspectives in millimeter wave frequencies using meta-heuristic algorithms," *Electronics*, vol. 8, no. 11, p. 1318.

[52] G. Fahira, A. Hikmaturokhman, and A. R. Danisya, (2020: IEEE)."5G NR Planning at mmWave Frequency: Study Case in Indonesia Industrial Area," in *2020 2nd International Conference on Industrial Electrical and Electronics (ICIEE)*,pp. 205-210.

[53] T. B. a. R.W.Heath, (2015)."Coverage and rate analysis for millimeter-wave cellular networks," *IEEE Transactions on Wireless Communications*, vol. Vol. 14, No. 2, pp. pp. 1100-1114.

[54] T. Bai, R. Vaze, and R. W. Heath, (2014)."Analysis of blockage effects on urban cellular networks," *IEEE Transactions on Wireless Communications*, vol. 13, no. 9, pp. 5070-5083.

[55] M. R. Akdeniz *et al.*, (2014)."Millimeter wave channel modeling and cellular capacity evaluation," *IEEE journal on selected areas in communications,* vol. 32, no. 6, pp. 1164-1179.

[56] S. Singh, M. N. Kulkarni, A. Ghosh, and J. G. Andrews, (2015)."Tractable model for rate in self-backhauled millimeter wave cellular networks," *IEEE Journal on Selected Areas in Communications,* vol. 33, no. 10, pp. 2196-2211.

[57] M.D.renzo, (2015)."Stochastic geometry modeling and analysis of multi-tier millimeter wave cellular networks," *IEEE Transactions on Wireless Communications,* vol. Vol. 14, no. No.19, pp. pp. 5038-5057.

[58] M. K. S. Singh, A. Ghosh, and J. G. Andrews, (2015)."Tractable model for rate in selfbackhauled millimeter wave cellular networks," *IEEE Journal on Selected Areas in Communications,,* vol. Vol. 33, no. No. 10, pp. pp. 2196-2211.

[59] S. Sun, (2017). "NYUSIM User Manual," *New York University, New York*.

[60] Y. Azar *et al.*, (2013: IEEE)."28 GHz propagation measurements for outdoor cellular communications using steerable beam antennas in New York City," in *2013 IEEE international conference on communications (ICC),* 2 pp. 5143-5147.

[61] C. Umit Bas *et al.*, (2017)."28 GHz Microcell Measurement Campaign for Residential Environment," *arXiv e-prints,* p. arXiv: 1711.00170.